Interferon lambda restricts herpes simplex virus skin disease by suppressing neutrophil-mediated pathology

Running Title: IFN-λ protects mice from severe HSV skin disease

Drake T. Philip[a], Nigel M. Goins[a], Nicholas J. Catanzaro[b], Ichiro Misumi[c], Jason K. Whitmire[ac], Hannah M. Atkins[d], Helen M. Lazear[a,#]

[a]Department of Microbiology & Immunology, University of North Carolina at Chapel Hill
[b]Department of Epidemiology, School of Public Health, University of North Carolina at Chapel Hill
[c]Department of Genetics, University of North Carolina at Chapel Hill
[d]Department of Pathology and Laboratory Medicine, University of North Carolina at Chapel Hill

[#]Corresponding author: helen.lazear@med.unc.edu

Word count (Abstract): 174
Word count (Text): 10015

ABSTRACT

Type III interferons (IFN-λ) are antiviral and immunomodulatory cytokines that have been best characterized in respiratory and gastrointestinal infections, but the effects of IFN-λ against skin infections have not been extensively investigated. We sought to define the skin-specific effects of IFN-λ against the highly prevalent human pathogen herpes simplex virus (HSV). We infected mice lacking the IFN-λ receptor (*Ifnlr1*$^{-/-}$), both the IFN-λ and the IFN-αβ receptor (*Ifnar1*$^{-/-}$ *Ifnlr1*$^{-/-}$), or IFN-λ cytokines (*Ifnl2/3*$^{-/-}$) and found that IFN-λ restricts the severity of HSV-1 and HSV-2 skin lesions, independent of a direct effect on viral load. Using conditional knockout mice, we found that IFN-λ signaling in both keratinocytes and neutrophils was necessary to control HSV-1 skin lesion severity, and that IFN-λ signaling in keratinocytes suppressed CXCL9-mediated neutrophil recruitment to the skin. Furthermore, depleting neutrophils or blocking CXCL9 protected against severe HSV-1 skin lesions in *Ifnlr1*$^{-/-}$ mice. Altogether, our results suggest that IFN-λ plays an immunomodulatory role in the skin that restricts neutrophil-mediated pathology during HSV infection, and suggest potential applications for IFN-λ in treating viral skin infections.

INTRODUCTION

The skin is one of the largest physiologic and immunologic barriers that separates the host from its environment and continuously encounters commensal and pathogenic microbes. Dysregulation of this barrier can result in inflammatory skin conditions, such as atopic dermatitis (eczema), or susceptibility to viral, bacterial, and fungal infections (Handfield et al., 2018). Resident and infiltrating immune cells as well as barrier-specific cytokines contribute to providing a balanced immune response in the skin (Nestle et al., 2009). The skin is comprised of two layers: the epidermis and dermis. The epidermis primarily consists of keratinocytes (skin epithelial cells) and T cells (CD8 and γδ). Keratinocytes form the physical barrier of the skin but also are immunologically active, coordinating resident and infiltrating leukocyte responses (Nestle et al., 2009). The dermis is primarily made of fibroblasts and is surveyed by a more diverse set of

immune cells including macrophages, dendritic cells, granulocytes, Langerhans cells, and T cells (CD8, CD4, γδ) (Nestle et al., 2009). Both layers of the skin act in concert to mediate immune responses, using a variety of cytokines and chemokines—including interferons (IFNs)—in balancing pathogen clearance with homeostasis and barrier integrity (Kobayashi et al., 2019).

There are three families of IFNs: type I (IFN-α/β), type II (IFN-γ), and type III (IFN-λ), which are distinguished by their receptor usage (Mesev et al., 2019). IFN-α/β and IFN-γ typically mediate systemic antiviral and immunomodulatory functions whereas the activity of IFN-λ is most evident at epithelial barriers such as the respiratory and gastrointestinal tracts (Lazear et al., 2019). There are four IFN-λ subtypes in humans (IFN-λ1-4), whereas mice express only IFN-λ2 and IFN-λ3 (Lazear et al., 2019). All IFN-λ subtypes signal through the same heterodimeric receptor comprised the IFNLR1 and IL10Rβ subunits (Dowling & Forero, 2022). IFN-λ intracellular signaling is similar to IFN-α/β in that upon receptor binding Jak1 and Tyk2 are activated to phosphorylate STAT1 and STAT2, which bind to IRF9 and translocate to the nucleus to drive interferon stimulated gene (ISG) expression (Dowling & Forero, 2022). Although IFN-λ and IFN-α/β canonically share the same intracellular signaling cascade and activate similar antiviral transcriptional programs, there has been a growing appreciation for their different antiviral and immunomodulatory functions. Their difference in function is in part due to kinetics, as IFN-α/β is induced more rapidly upon infection whereas IFN-λ is produced later and for longer throughout infection (Lazear et al., 2019; Mesev et al., 2019). Further, whereas the IFN-α/β receptor (IFNAR1/IFNAR2 heterodimer) is expressed ubiquitously, IFNLR1 expression is restricted primarily to epithelial cells and select leukocytes such as neutrophils, dendritic cells, and macrophages (Lazear et al., 2019). The high expression of IFNLR in epithelial tissues has led to substantial characterization of IFN-λ antiviral and immunomodulatory functions at epithelial barriers including the respiratory tract and gastrointestinal tract. However, relatively little is known about the role of IFN-λ in the skin, even though the skin is an important epithelial barrier and home to a variety of IFN-λ producing and responding cell types.

Therefore, we sought to investigate the functions of IFN-λ signaling in the skin using a highly prevalent human skin pathogen, herpes simplex virus (HSV-1 and HSV-2). HSV-1 primarily manifests as orofacial or genital lesions but severe complications of HSV-1 infection include herpes encephalitis, herpes keratitis, and eczema herpeticum (Kollias et al., 2015). HSV-2 most commonly causes genital herpes and can cause severe disease when transmitted to neonates at delivery (Bradley et al., 2014). HSV-1 and HSV-2 establish life-long persistent (latent) infections in sensory neurons that are never cleared by the immune system; viral reactivation from latency results in recurrent epithelial lesions (cold sores, genital herpes) and transmission to new individuals. Over half of the US adult population are seropositive for HSV-1 and 15% are seropositive for HSV-2 (Bradley et al., 2014). The disease associated with HSV-1 infection, in both mice and humans, is partly immune-mediated (Kollias et al., 2015) but the viral and host factors that drive disease severity are not fully understood, including the effects of IFN-λ signaling in HSV-1 skin infection.

Here, we report a protective role for IFN-λ signaling in restricting severe HSV-1 skin disease. Using a mouse model of HSV-1 skin infection, we found that IFN-λ-dependent protection from severe HSV-1 skin disease requires signaling in both keratinocytes and leukocytes (including neutrophils). We found that neutrophils are the primary leukocytes recruited to the skin during HSV-1 infection, and that mice lacking IFN-λ signaling (*Ifnlr1*$^{-/-}$) have more skin-infiltrating neutrophils compared to wild-type mice. We found a greater proportion of neutrophils expressing the tissue homing integrin leukocyte function associated antigen- 1 (LFA-1) in *Ifnlr1*$^{-/-}$ compared to wild-type mice, suggesting that *Ifnlr1*$^{-/-}$ neutrophils are highly recruited to and retained in HSV-1 infected skin. Furthermore, we showed that depleting neutrophils prevented the development of severe HSV-1 skin lesions in *Ifnlr1*$^{-/-}$ mice and that IFN-λ signaling in keratinocytes limits CXCL9-mediated neutrophil recruitment to the skin. Altogether, our results suggest that IFN-λ plays an immunomodulatory role in the skin that restricts neutrophil-mediated pathology during HSV infection and suggest potential applications for IFN-λ in treating viral skin infections.

RESULTS

Defining HSV-1 skin lesion severity in the mouse flank infection model

Flank scarification is a well-established mouse model for studying HSV-1 pathogenesis (Simmons & Nash, 1984; van Lint et al., 2004; Wang et al., 2019). In the standard model, HSV-1 is scratched into depilated flank skin using a 27 gauge needle (Simmons & Nash, 1984; van Lint et al., 2004; Wang et al., 2019). The virus replicates at the inoculation site, infects innervating sensory neurons and traffics in a retrograde direction to the neuron cell body located in the dorsal root ganglia (DRG), then traffics in an anterograde direction, returning to the entire dermatome innervated by that DRG, producing a dermatome skin lesion (Fig. S1A) (Wang et al., 2019). To improve the reproducibility of this infection model, we tested two modifications to the commonly used procedures. First, we depilated mice by manual plucking, rather than shaving plus chemical depilation (e.g. Nair cream). Plucking re-sets the hair cycle (Kobayashi et al., 2019), producing an immunologically uniform environment across the depilated skin, and also is faster and easier than shaving plus chemical depilation. We found no significant difference in dermatome lesion area for mice depilated by plucking compared to shaving plus Nair (Fig. S1B), suggesting that the method of depilation does not impact HSV-1 skin infection in this model, so further experiments depilated mice by plucking. Next, we compared three methods for disrupting the skin barrier, as HSV-1 does not efficiently infect intact skin. We applied 10^6 focus-forming units (FFU) of HSV-1 (strain NS) onto depilated flank skin and abraded the inoculation site skin by i) 40 gentle scratches with a 27G needle, ii) 10 closely-spaced punctures with a Quintip skin test (allergy needle), or iii) a single puncture with a Greer pick skin test, and measured viral loads in dermatome skin at 6 days post-infection (dpi). We found that skin viral loads corresponded to the extent of skin barrier disruption, with needle scarification producing a higher median viral load than a Quintip puncture (5.0 vs. 4.2 Log_{10} FFU/g) and no virus detected after a Greer pick puncture (Fig. S1C). Although needle scarification produced higher median viral loads, there was greater mouse-to-mouse

variability compared to Quintip puncture (standard deviation (SD) 1.1 vs 0.7 Log_{10} FFU/g) and we and others have observed substantial operator-to-operator variability with needle scarification. Further, we found no difference in median lesion area between needle scarification and Quintip puncture (Fig. S1D); therefore, we used Quintip puncture to disrupt the skin barrier for further experiments.

We also sought to define a categorical system for classifying dermatome lesions as mild, moderate, or severe to better describe skin lesion phenotypes. We infected 20 wild-type mice with HSV-1, measured dermatome lesion area at 6 dpi, and found a mean area of 11 mm^2 (SD 12 mm^2) (Fig. S1E). We defined severe lesions as those with area >1 SD above the mean (>23 mm^2), mild lesions as those with area smaller than the average size of the inoculation site (<5 mm^2), and moderate lesions as 5-23 mm^2 (Fig. S1F-G). We used both lesion area and categorical severity score to assess dermatome lesions in further experiments. Altogether, the flank infection model provides a robust system for assessing HSV-1 pathogenesis in the skin.

IFN-λ signaling protects mice from severe HSV skin disease

IFN-λ provides antiviral protection at epithelial barriers such as the respiratory and gastrointestinal tracts (Broggi et al., 2020), but the effects of IFN-λ on viral infection in the skin have not been extensively investigated. To address this gap in the field, we infected wild-type mice and mice that lack the IFN-λ receptor (*Ifnlr1*$^{-/-}$) with 10^6 FFU of HSV-1 and evaluated skin lesion area, severity, and viral load 2-10 dpi (Fig. 1A-D). Experimental mice were generated by crossing mice with a floxed allele of the IFN-λ receptor (*Ifnlr1*$^{f/f}$) with mice hemizygous for Cre recombinase expression under a ubiquitous promoter (*ActB*-Cre), producing littermate Cre- (wild-type) and Cre+ (*Ifnlr1*$^{-/-}$) mice. Genotyping was performed retrospectively after data analysis and experiments were conducted blinded to the *Ifnlr1* status of each mouse. We found that *Ifnlr1*$^{-/-}$ mice developed significantly larger skin lesions than wild-type mice at 6 dpi, the time of peak

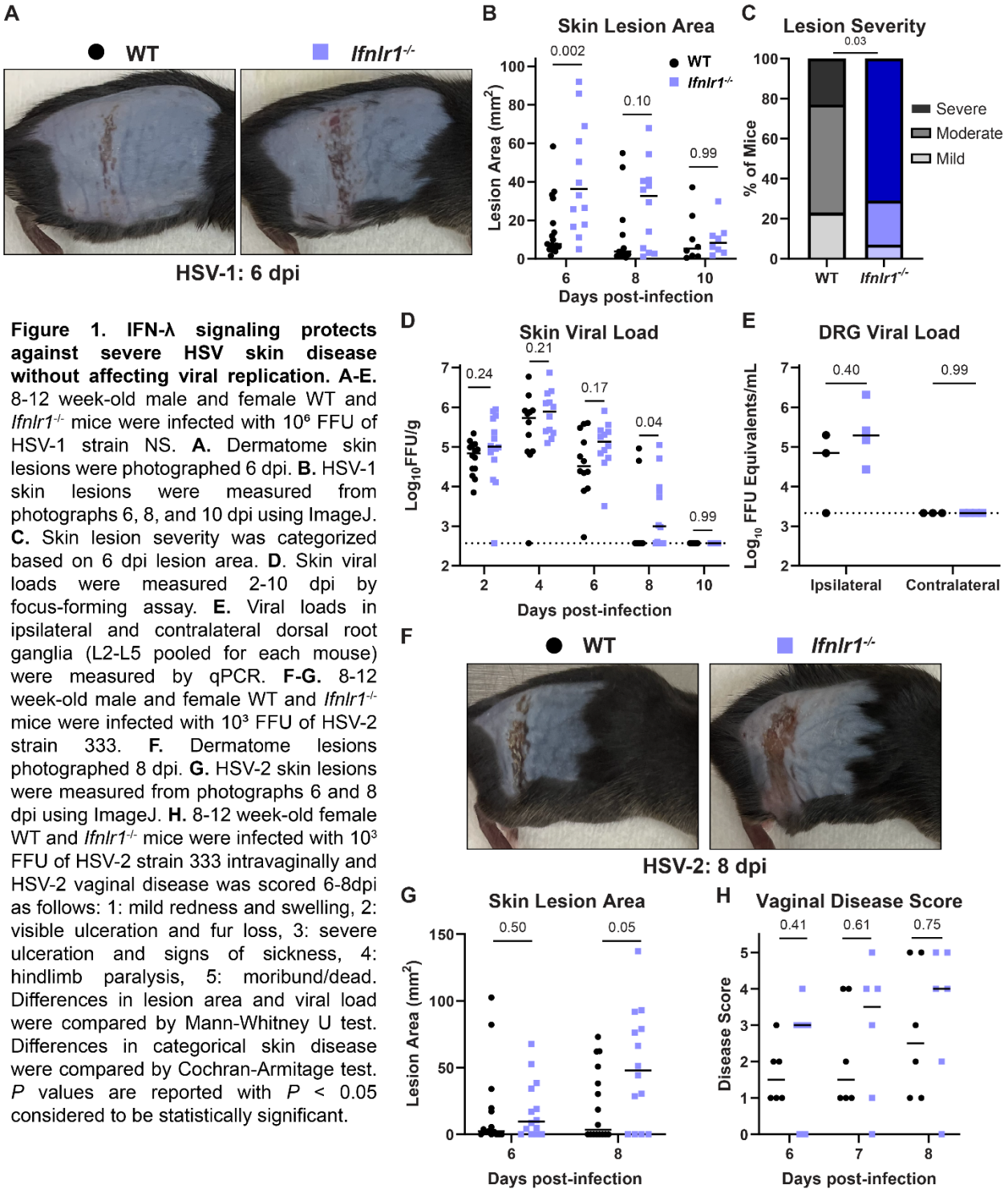

Figure 1. IFN-λ signaling protects against severe HSV skin disease without affecting viral replication. A-E. 8-12 week-old male and female WT and *Ifnlr1*$^{-/-}$ mice were infected with 10^6 FFU of HSV-1 strain NS. **A.** Dermatome skin lesions were photographed 6 dpi. **B.** HSV-1 skin lesions were measured from photographs 6, 8, and 10 dpi using ImageJ. **C.** Skin lesion severity was categorized based on 6 dpi lesion area. **D.** Skin viral loads were measured 2-10 dpi by focus-forming assay. **E.** Viral loads in ipsilateral and contralateral dorsal root ganglia (L2-L5 pooled for each mouse) were measured by qPCR. **F-G.** 8-12 week-old male and female WT and *Ifnlr1*$^{-/-}$ mice were infected with 10^3 FFU of HSV-2 strain 333. **F.** Dermatome lesions photographed 8 dpi. **G.** HSV-2 skin lesions were measured from photographs 6 and 8 dpi using ImageJ. **H.** 8-12 week-old female WT and *Ifnlr1*$^{-/-}$ mice were infected with 10^3 FFU of HSV-2 strain 333 intravaginally and HSV-2 vaginal disease was scored 6-8dpi as follows: 1: mild redness and swelling, 2: visible ulceration and fur loss, 3: severe ulceration and signs of sickness, 4: hindlimb paralysis, 5: moribund/dead. Differences in lesion area and viral load were compared by Mann-Whitney U test. Differences in categorical skin disease were compared by Cochran-Armitage test. *P* values are reported with $P < 0.05$ considered to be statistically significant.

disease (median lesion area 36.2 vs 7.7 mm^2, P <0.01; Fig. 1B), and that a greater proportion of *Ifnlr1*$^{-/-}$ mice developed severe skin lesions compared to wild-type mice (71% vs 23%, $P < 0.05$; Fig. 1C). There was no significant difference in lesion area between *Ifnlr1*$^{-/-}$ and wild-type mice at

8 or 10 dpi (Fig. 1B). We measured viral loads by focus-forming assay from *Ifnlr1*$^{-/-}$ and wild-type skin lesions and from infected skin prior to lesion development (Fig. 1D). We found no significant differences in skin viral load between *Ifnlr1*$^{-/-}$ and wild-type mice at 2, 4, or 6 dpi (Fig. 1D), suggesting that IFN-λ signaling does not restrict HSV-1 replication in the skin. *Ifnlr1*$^{-/-}$ mice sustained detectable viral loads in the skin longer than wild-type mice (8 of 12 *Ifnlr1*$^{-/-}$ mice positive at 8 dpi vs 2 of 12 wild-type mice, $P < 0.05$), but *Ifnlr1*$^{-/-}$ and wild-type mice both cleared the infection from the skin by 10 dpi (Fig. 1D). To determine whether differences in dermatome skin lesions resulted from differences in sensory neuron infection, we infected wild-type and *Ifnlr1*$^{-/-}$ mice, harvested DRG at 6 dpi, and quantified viral loads by qPCR. We found no significant differences in HSV-1 viral genomes in DRG 6 dpi (Fig. 1E). Altogether, these results suggest that IFN-λ restricts HSV-1 skin lesion severity independently of a direct effect on viral replication.

We next tested whether IFN-λ had a similar protective effect against skin lesions caused by HSV-2. We infected mice with 1000 FFU of HSV-2 (strain 333) and measured dermatome lesion areas 6 and 8 dpi (Fig. 1F-G). The kinetics of HSV-2 infection were slower, with peak skin lesion area at 8 dpi, compared to 6 dpi for HSV-1, even though HSV-2 (333) was more virulent than HSV-1 (NS) (~75% mortality at an inoculation dose of 1000 FFU of HSV-2 (333) compared to ~0% mortality at an inoculation dose of 10^6 FFU of HSV-1 (NS). Similar to HSV-1, *Ifnlr1*$^{-/-}$ mice developed significantly larger lesions compared to wild-type mice (median lesion area at 8 dpi 47.8 mm^2 vs 3.6 mm^2, $P < 0.05$; Fig. 1G). Despite the slower kinetics of HSV-2 skin disease, the peak area of HSV-2 lesions in *Ifnlr1*$^{-/-}$ mice was larger than HSV-1 lesions (median lesion area 47.8 mm^2 at 8 dpi vs 36.2 mm^2 at 6 dpi; Fig. 1B and 1G). We next asked whether IFN-λ protected against HSV disease at other epithelial sites. Although both HSV-1 and HSV-2 infect the genital tract in humans and mice, HSV-1 does not cause overt vaginal disease in mice. Therefore, we used HSV-2 to assess the effects of IFN-λ during vaginal infection. We found no significant difference between *Ifnlr1*$^{-/-}$ and wild-type vaginal disease severity 6-8 dpi (Fig. 1H). After 8 dpi, mice either began to recover or were euthanized due to neurologic disease signs (hindlimb

paralysis and hunching). Altogether these results show that IFN-λ protects against severe skin disease caused by both HSV-1 and HSV-2.

The protective effect of IFN-λ in the skin does not require IFN-α/β signaling

IFN-λ and IFN-αβ signal through distinct receptors but canonically activate an overlapping JAK/STAT signaling cascade and transcriptional response (Dowling & Forero, 2022). To determine whether the protective effects of IFN-λ in the skin acted via cross-talk with IFN-α/β signaling, we infected mice lacking the IFN-αβ receptor (*Ifnar1*$^{-/-}$) or both the IFN-αβ and IFN-λ receptors (*Ifnar1*$^{-/-}$ *Ifnlr1*$^{-/-}$ double-knockout, DKO) with HSV-1 and evaluated survival, skin lesion area, severity, and viral loads (Fig. 2A-E). As expected, in the absence of IFN-αβ signaling, the

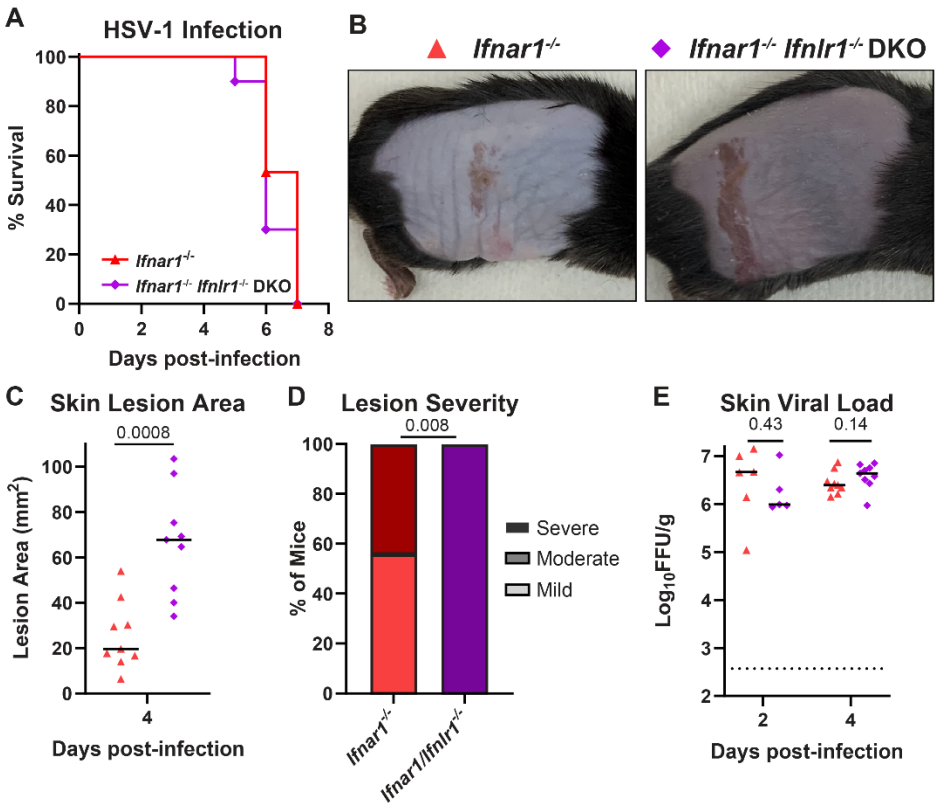

Figure 2. The protective effect of IFN-λ in the skin does not require IFN-α/β signaling. 8-12 week-old *Ifnar1*$^{-/-}$ and *Ifnar1*$^{-/-}$ *Ifnlr1*$^{-/-}$ DKO male and female mice were infected with 10^6 FFU of HSV-1. **A.** Lethality was monitored daily (n=15 *Ifnar1*$^{-/-}$ and 10 DKO mice). **B.** Dermatome skin lesions were photographed 4 dpi. **C.** Skin lesion areas were measured from photographs 4 dpi using ImageJ. **D.** Skin lesion severity was categorized based on 4 dpi lesion area. **E.** Skin viral loads were measured 2 and 4 dpi by focus-forming assay. Survival differences were compared by Mantel-Cox Log-Rank test. Differences in lesion area and viral load were compared by Mann-Whitney U test and differences in categorical skin disease were compared by Cochran-Armitage test. *P* values are reported with $P < 0.05$ considered to be statistically significant.

kinetics of HSV-1 infection were faster and disease was more severe, with all mice succumbing 5-8 dpi (Fig. 2A). At 4 dpi, the first day mice developed lesions, *Ifnar1*$^{-/-}$ *Ifnlr1*$^{-/-}$ DKO mice developed significantly larger skin lesions compared to *Ifnar1*$^{-/-}$ mice (median lesion area 67.8 mm^2 vs 19.7 mm^2, $P < 0.001$; Fig. 2B-C) and a significantly larger proportion developed severe lesions (100% vs. 44%, $P < 0.001$; Fig. 2D). We found no significant difference in skin viral loads at 2 dpi or 4 dpi (Fig. 2E). Altogether, these data indicate that IFN-λ limits severe HSV-1 skin disease independently of IFN-α/β and independent of a direct antiviral effect on HSV-1 replication in the skin.

IFN-λ cytokines protect against severe HSV-1 skin disease

We next asked which cell types produced the IFNs responsible for controlling HSV-1 skin disease. To determine whether mice lacking IFN-λ cytokines recapitulate the phenotype of mice lacking the IFN-λ receptor, we infected mice lacking IFN-λ2 and IFN-λ3 (*Ifnl2/3*$^{-/-}$), the only IFN-λ cytokines produced in mice (Peterson et al., 2019), and measured skin lesion area, disease severity, and skin viral loads (Fig. 3A-D). At 6 dpi, *Ifnl2/3*$^{-/-}$ mice developed significantly larger skin lesions compared to wild-type mice (median area 20.2 mm^2 vs 7.1 mm^2, $P < 0.01$; Fig. 3B), and a significantly higher proportion of *Ifnl2/3*$^{-/-}$ mice developed severe skin lesions compared to wild-type mice (45% vs 15%, $P < 0.01$, Fig. 3C) with no significant difference in skin viral loads (Fig. 3D). Altogether, the phenotype of mice lacking IFN-λ cytokines was consistent with the phenotype of mice lacking the IFN-λ receptor, providing an independent line of evidence that IFN-λ signaling restricts severe HSV-1 skin disease.

Although some type I IFNs, such as IFN-α and IFN-β, can be produced by many cell types, IFN-κ is a type I IFN that is thought to be produced predominantly by keratinocytes (Gharaee-Kermani et al., 2022; LaFleur et al., 2001). To determine whether a keratinocyte-specific type I IFN might play a role in role in controlling skin disease caused by HSV-1, we infected *Ifnk*$^{-/-}$ mice. We found no significant differences in lesion area, disease severity, or skin viral loads between

210 *Ifnk*$^{-/-}$ mice and wild-type mice (Fig. 3A-D), suggesting that, despite its keratinocyte-specific

211 nature, IFN-κ does not play a key role controlling HSV-1 infection in the skin.

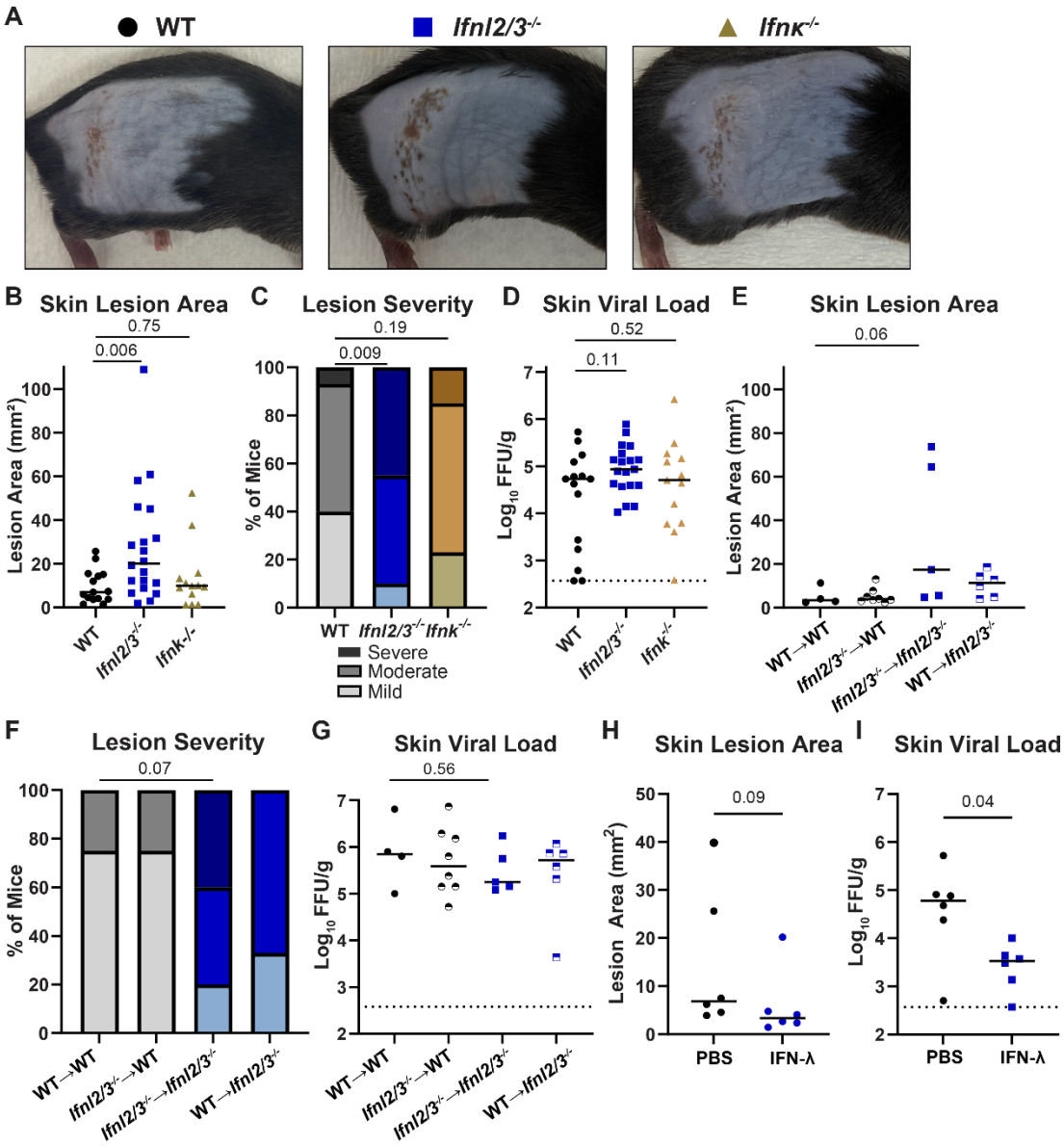

Figure 3. IFN-λ cytokines protect against severe HSV-1 skin disease. A-D. 8-12 week-old WT, *Ifnl2/3*$^{-/-}$, and *Ifnk*$^{-/-}$ male and female mice were infected with 10^6 FFU of HSV-1. **A.** Dermatome skin lesions were photographed 6 dpi. **B.** Skin lesion areas were measured from photographs 6 dpi using ImageJ. **C.** Skin lesion severity was categorized based on 6 dpi lesion area. **D.** Skin viral loads were measured 6 dpi by FFA. **E-G.** 8 week-old WT and *Ifnl2/3*$^{-/-}$ male and female mice were lethally irradiated and transfused with 10^7 bone marrow cells from WT or *Ifnl2/3*$^{-/-}$ donors. 10 weeks later, mice were infected with 10^6 FFU of HSV-1. **E.** Skin lesion areas were measured from photographs 6 dpi using ImageJ. **F.** Skin lesion severity was categorized based upon 6 dpi lesion area. **G.** Skin viral loads were measured 6 dpi by FFA. **H-I.** 8-12 week-old WT male and female mice were depilated and then topically treated with 5 μg of recombinant murine IFN-λ3 or PBS. 24 hours later, mice were infected with 10^6 FFU of HSV-1 at the treated site. **H.** Skin lesion areas were measured from photographs 6 dpi using ImageJ. **I.** Skin viral loads were measured 6 dpi by FFA. Differences in lesion area and viral load were compared by Mann-Whitney U test and differences in categorical skin disease were compared by Cochran-Armitage test. *P* values are reported with $P < 0.05$ considered to be statistically significant.

To determine the source of protective IFN-λ during HSV-1 skin infection, we used bone marrow chimeras between wild-type and *Ifnl2/3*$^{-/-}$ mice, generating mice that lacked the ability to produce IFN-λ2/3 in either their hematopoietic or stromal compartments. Due to a lack of antibodies to detect IFN-λ, we used PCR genotyping to confirm effective bone marrow engraftment in recipients. We then infected IFN-λ chimeric mice with HSV-1 and evaluated skin disease 6 dpi (Fig 3E). *Ifnl2/3*$^{-/-}$ mice receiving *Ifnl2/3*$^{-/-}$ bone marrow showed a trend toward larger lesions and more severe disease than wild-type mice receiving wild-type bone marrow (median area 17.3 mm^2 vs 3.5 mm^2, $P = 0.06$; Fig. 3E), consistent with our observations in non-irradiated mice. However, we found that mice retaining IFN-λ production in either their hematopoietic compartment or their stromal compartment were protected from severe HSV-1 skin disease (Fig. 3F), suggesting that multiple cell types can produce protective IFN-λ during HSV-1 skin infection. As in our previous experiments, the effects of IFN-λ on skin lesion severity were independent of an effect on viral load (Fig. 3G).

Exogenous IFN-λ treatment has shown therapeutic potential against various viral infections and autoimmune diseases (Blazek et al., 2015; Dinnon et al., 2020; Feld et al., 2021; Flisiak et al., 2016; Muir et al., 2014), therefore, we sought to determine whether topical administration of IFN-λ could limit HSV-1 infection and skin lesions. We depilated mice two days prior to infection, pretreated topically with 5 μg of IFN-λ and infected with HSV-1 on the treated site one day later. We found a modest decrease in lesion areas in IFN-λ pretreated mice at 6 dpi compared to PBS-pretreated mice (median area 3.4 mm^2 vs 6.9 mm^2, $P = 0.09$; Fig. 3G). Additionally, we found that viral loads at 6 dpi were significantly reduced in IFN-λ pretreated mice compared to PBS-pretreated mice (median viral load 3.53 Log_{10} FFU/g vs 4.78 Log_{10} FFU/g, $P < 0.05$; Fig. 3H). Altogether, these data indicate that exogenous prophylactic administration of IFN-λ can limit severe HSV-1 skin disease, suggesting potential opportunities for therapeutic interventions.

IFN-λ signaling in both keratinocytes and leukocytes is necessary to restrict severe HSV-1 skin disease

The skin is comprised of diverse cell types including keratinocytes and resident and infiltrating leukocytes. To determine which IFN-λ responsive cell types contribute to controlling HSV-1 skin infection, we used conditional knockout mice lacking IFN-λ signaling in keratinocytes (*K14*-Cre-*Ifnlr1*$^{-/-}$) or leukocytes (*Vav*-Cre-*Ifnlr1*$^{-/-}$). These mice were bred as Cre hemizygotes, generating littermate Cre- controls (wild-type) and were genotyped retrospectively, allowing experiments to be performed blinded to the *Ifnlr1* status of each mouse. *Vav*-Cre-*Ifnlr1*$^{-/-}$ mice have been previously reported (Baldridge et al., 2017; Casazza et al., 2022); however, to our knowledge this is the first derivation of *K14*-Cre-*Ifnlr1*$^{-/-}$ mice. To validate conditional depletion of the *Ifnlr1* in these mice, we used PCR genotyping in specific tissues in wild-type (Cre-) and *K14*-Cre-*Ifnlr1*$^{-/-}$ (Cre+) mice and found Cre-mediated rearrangement of the *Ifnlr1*$^{f/f}$ allele only in epithelial tissues (Fig. S2). Conditional knockout mice were compared to *Ifnlr1*$^{-/-}$ mice generated by crossing *Ifnlr1*$^{f/f}$ mice to mice expressing Cre recombinase under a CMV promoter and subsequently bred as knockout x knockout.

We infected wild-type, *Ifnlr1*$^{-/-}$, *K14*-Cre-*Ifnlr1*$^{-/-}$, and *Vav*-Cre-*Ifnlr1*$^{-/-}$ mice with HSV-1 and evaluated skin lesion area, disease severity, and viral loads 6 dpi (Fig. 4A-D). We found that *Ifnlr1*$^{-/-}$ mice developed significantly larger lesions than wild-type mice (median area 13.1 mm^2 vs 6.7 mm^2, $P < 0.01$) (Fig. 4B) and a greater proportion of these mice developed severe skin disease (34% vs 14%, $P < 0.01$) (Fig. 4C), further supporting a role for IFN-λ in controlling severe HSV-1 skin disease in an independent line of *Ifnlr1*$^{-/-}$ mice compared to those used in our earlier experiments (Fig. 1). We found that mice lacking IFN-λ signaling exclusively in keratinocytes or in leukocytes developed skin lesions similar in size to *Ifnlr1*$^{-/-}$ mice (median area 15.7 mm^2, 14.6 mm^2, and 13.1 mm^2, $P > 0.05$) (Fig. 4C) and a similar proportion developed severe lesions (40%, 44%, 34%, $P > 0.05$) (Fig. 4D). We found no significant differences in skin viral loads comparing *Ifnlr1*$^{-/-}$ mice to wild-type or comparing conditional knockouts to *Ifnlr1*$^{-/-}$ (Fig. 4D). Altogether, these

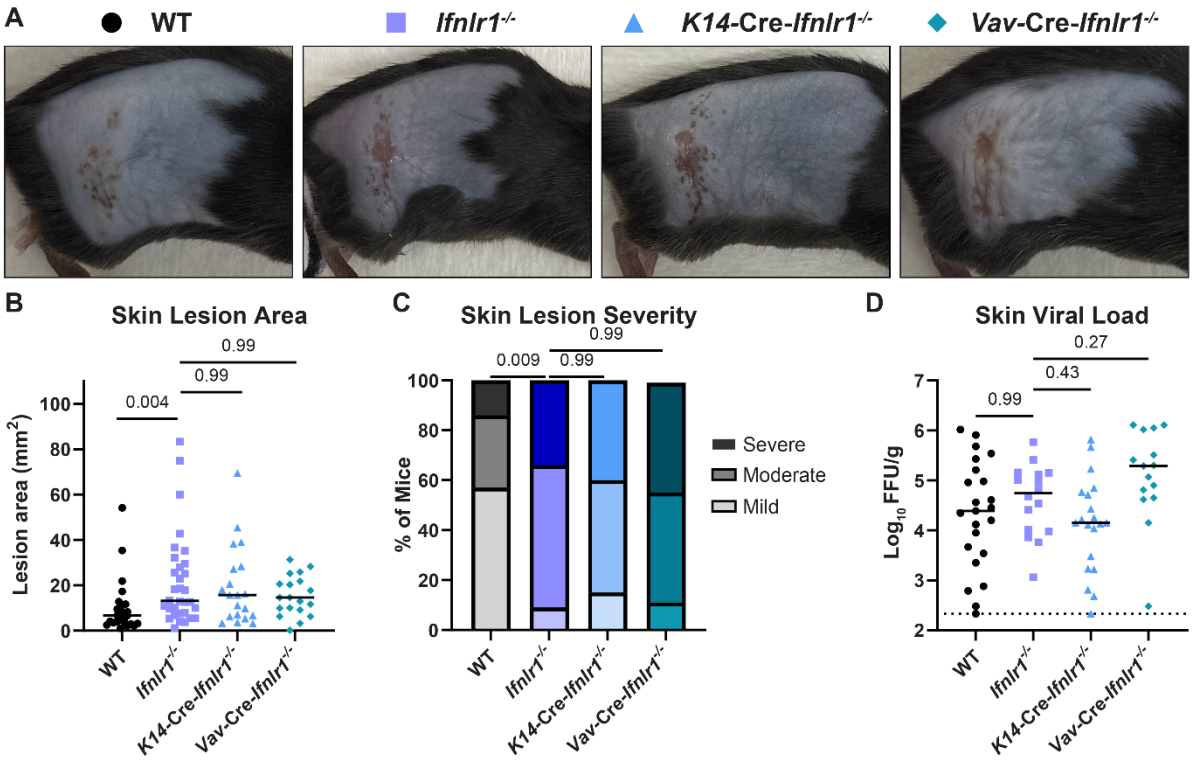

Figure 4. IFN-λ signaling in both keratinocytes and leukocytes is necessary to restrict severe HSV-1 skin disease. 8-12 week-old male and female WT, *Ifnlr1*$^{-/-}$, *K14*-Cre-*Ifnlr1*$^{-/-}$, and *Vav*-Cre-*Ifnlr1*$^{-/-}$ mice were infected with 10^6 FFU of HSV-1. **A.** Dermatome skin lesions photographed were 6 dpi. B. Skin lesion areas were measured from photographs 6 dpi using ImageJ. **C.** Skin lesion severity was categorized based on 6 dpi lesion area. **D.** Skin viral loads were measured 6 dpi by FFA. Differences in lesion area and viral load were compared by Mann-Whitney U test and differences in categorical skin disease were compared by Cochran-Armitage test. *P* values are reported with $P < 0.05$ considered to be statistically significant.

data indicate that IFN-λ signaling in both keratinocytes and leukocytes is necessary to control severe HSV-1 skin disease.

IFN-λ signaling in keratinocytes differentially regulates inflammatory genes, including CXCL9

Because we found that IFN-λ signaling in both keratinocytes and leukocytes was necessary to control HSV-1 skin lesion severity, we next asked whether this was due to crosstalk between keratinocytes and leukocytes. To understand how IFN-λ could be mediating signaling between epithelial cells and immune cells, we first generated IFN receptor knockout A549 cells, a human lung epithelial cell line. We treated *IFNLR1* KO, *IFNAR1* KO, or nontargeting control (RenLuc) A549 cells with recombinant IFN-β or IFN-λ and measured induction of the ISG *IFIT1* by qRT-PCR. As expected, *IFNLR1* KO cells responded to IFN-β but not IFN-λ and *IFNAR1* KO cells responded to IFN-λ but not IFN-β (Fig. S4A). We then treated control and IFN receptor KO

cells with 50 ng/mL IFN-λ, 5 ng/mL IFN-β, or media alone for 8 hours and performed bulk RNAseq (Fig. S4B-F). We found that the transcriptional response after IFN-λ treatment in A549 cells was modest compared to IFN-β (Supplementary Table 1), consistent with prior studies (Coldbeck-Shackley et al., 2023; Zhou et al., 2007). However, prior studies that used primary cells rather than cell lines found more robust transcriptional responses induced by IFN-λ (Caine et al., 2019; Galani et al., 2017). We therefore investigated IFN-λ induced transcriptional responses in primary keratinocytes.

To define the IFN-λ specific response in keratinocytes and understand how IFN-λ could be signaling through keratinocytes to mediate their crosstalk with leukocytes, we generated primary keratinocytes from wild-type, *Ifnar1*$^{-/-}$, *Ifnlr1*$^{-/-}$, and *Ifnar1*$^{-/-}$ *Ifnlr1*$^{-/-}$ DKO mice, and treated them with 5 ng IFN-λ, 5 ng IFN-β, or media for 24 hours. We first measured induction of *Ifit1* by qRT-PCR. As expected, IFN-β did not induce a response in *Ifnar1*$^{-/-}$ cells, IFN-λ did not induce a response in *Ifnlr1*$^{-/-}$ cells, and neither IFN induced a response in *Ifnar1*$^{-/-}$ *Ifnlr1*$^{-/-}$ cells (Fig. 5A). We then performed bulk RNAseq with the goal of identifying IFN-λ-specific antiviral inflammatory mediators. By principal component analysis, triplicate samples clustered together, but different genotypes were distinct even without IFN treatment, suggesting differences in tonic IFN signaling in keratinocytes (Fig 5B). While the IFN-β response was largely unchanged in *Ifnlr1*$^{-/-}$ cells compared to wild-type, the IFN-λ response was diminished in *Ifnar1*$^{-/-}$ cells by both qRT-PCR (Fig. 5A) and principal component analysis (Fig. 5B), suggesting cross-talk between IFN-λ and IFN-β signaling in keratinocytes as well as in A549 cells (Fig. S4B). Although the IFN-λ response generally is reported to be less potent than the IFN-α/β response (Fig. S4) (Lazear et al., 2019), we found that many ISGs (including *Ifit1* and *Rsad2*) were induced to a similar magnitude by IFN-λ and IFN-β (Fig. 5A, C). We found a subset of ISGs in primary keratinocytes to be differentially induced by IFN-λ but not IFN-β (Fig. 5D). However, upon inspecting the IFN-λ-specific gene list

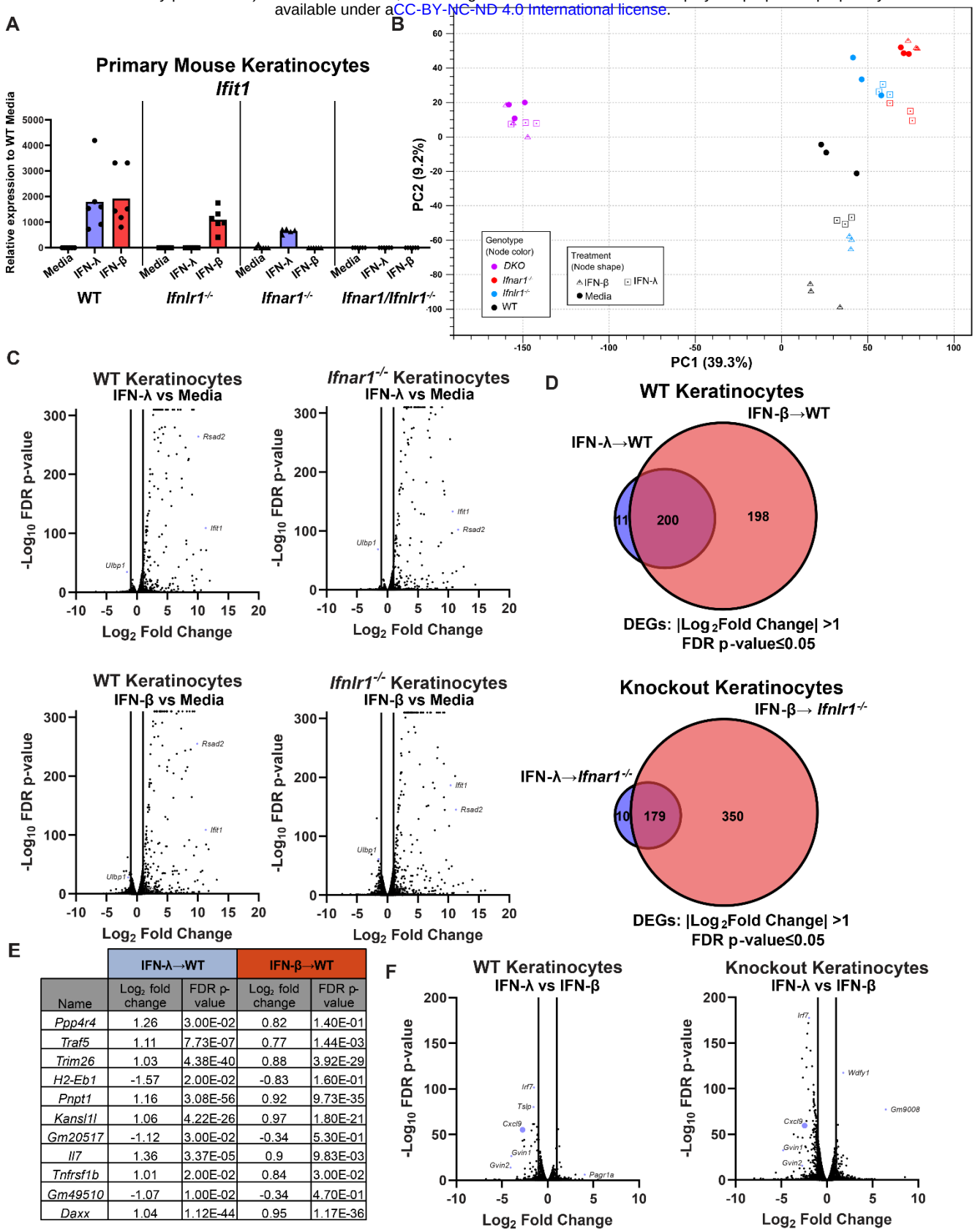

E

	IFN-λ→WT		IFN-β→WT	
Name	Log_2 fold change	FDR p-value	Log_2 fold change	FDR p-value
Ppp4r4	1.26	3.00E-02	0.82	1.40E-01
Traf5	1.11	7.73E-07	0.77	1.44E-03
Trim26	1.03	4.38E-40	0.88	3.92E-29
H2-Eb1	-1.57	2.00E-02	-0.83	1.60E-01
Pnpt1	1.16	3.08E-56	0.92	9.73E-35
Kansl1l	1.06	4.22E-26	0.97	1.80E-21
Gm20517	-1.12	3.00E-02	-0.34	5.30E-01
Il7	1.36	3.37E-05	0.9	9.83E-03
Tnfrsf1b	1.01	2.00E-02	0.84	3.00E-02
Gm49510	-1.07	1.00E-02	-0.34	4.70E-01
Daxx	1.04	1.12E-44	0.95	1.17E-36

Figure 5. IFN-λ signaling in keratinocytes differentially regulates CXCL9 induction. Primary keratinocytes were prepared from WT, *Ifnlr1*$^{-/-}$, *Ifnar1*$^{-/-}$ and *Ifnar1*$^{-/-}$ *Ifnlr1*$^{-/-}$ DKO mice and treated with IFN-λ3 (5 ng/mL), IFN-β (5 ng/mL), or media alone for 24 hours. **A.** RNA was extracted IFN-stimulated gene expression was measured by qRT-PCR. *Ifit1* expression is shown relative to *ActB* (housekeeping gene) and normalized to expression in media-treated WT cells. Results represent 6 samples from 2 independent experiments. **B-F.** RNA from 3 samples per genotype per treatment was analyzed by RNAseq (NovaSeq6000S4 XP Paired End 2x100). **B.** Principal component analysis for all analyzed samples. **C.** Volcano plots showing differentially expressed genes after IFN-λ or IFN-β treatment, compared to media-only treated keratinocytes. Differentially expressed genes were defined as having a |Log_2Fold Change| >1 and an FDR p-value ≤ 0.05. **D.** Venn diagram showing DEGs induced by IFN-λ and IFN-β in WT or knockout keratinocytes. **E.** Table of IFN-λ-specific DEGs, their Log_2Fold Change, and FDR p-value for IFN-λ and IFN-β-treated WT keratinocytes. **F.** Volcano plot showing DEGs after IFN-λ treatment compared to IFN-β treatment in WT and receptor knockout keratinocytes.

we found that while 11 or 10 genes did meet our differential threshold (2-fold change, FDR $P < 0.05$), these genes all were induced to a similar extent by IFN-β (although not quite reaching the differential threshold) (Fig. 5E). Moreover, none of the genes identified as IFN-λ-specific in wild-type or knockout keratinocytes overlapped (Supplementary Table 2), arguing against a set of ISGs that are induced in an IFN-λ specific manner in this system.

We next analyzed the IFN-λ response relative to the IFN-β response in WT and knockout keratinocytes to identify genes that are differentially regulated by IFN-λ compared to IFN-β (Fig. 5F). We found that the chemokine CXCL9 was one of the top differentially regulated genes between IFN-λ and IFN-β treatment in both wild-type and the corresponding receptor knockout keratinocytes. Notably, *Cxcl9* was significantly less induced after IFN-λ treatment compared to IFN-β in wild-type keratinocytes (9.7-fold vs 65.0-fold) and knockout keratinocytes (23.0-fold vs 58.5-fold). Because *Cxcl9* is known to recruit a variety of immune cells such as T cells, NK cells, and neutrophils (Chami et al., 2014, 2017; Karin, 2020), we next sought to characterize IFN-λ-dependent leukocyte changes in HSV-1 infected skin to identify possible players in IFN-λ-mediated protection by keratinocytes and leukocytes.

Skin lesions in Ifnlr1$^{-/-}$ mice exhibit extensive neutrophil infiltration and severe pathology

To define IFN-λ dependent changes in leukocyte populations in response to HSV-1 infection, we harvested skin lesions and adjacent healthy skin at 6 dpi from *Ifnlr1*$^{-/-}$ and wild-type mice and analyzed leukocyte populations by flow cytometry. We found no significant difference between *Ifnlr1*$^{-/-}$ and wild-type leukocyte population frequencies in the healthy skin at 6 dpi (Fig. S3A). Further, we found no differences in leukocyte frequency, including dendritic cells, macrophages, CD4 and CD8 T cells, B cells, or NK cells, between *Ifnlr1*$^{-/-}$ and wild-type skin lesions at 6 dpi (Fig. S3A). However, we found that skin lesions from *Ifnlr1*$^{-/-}$ mice exhibited a significantly higher frequency of neutrophils (CD45+CD11b+Ly6G+, Fig. 6A-B) compared to wild-type mice at 6 dpi (mean neutrophil frequency 21.1% vs 6.7%; Fig. 6B). Although we found a significant increase in γδT cells between *Ifnlr1*$^{-/-}$ and wild-type mice (Fig. S3A), we did not further

investigate these cells as they are not known to be IFN-λ responsive and are less abundant in the skin compared to neutrophils. This increase in neutrophil frequency was specific to the skin lesion, because in adjacent healthy skin neutrophil abundance was very low and there was no significant difference between *Ifnlr1*$^{-/-}$ and wild-type mice (Fig. 6B). The increase in neutrophil frequency in *Ifnlr1*$^{-/-}$ mice corresponded to the kinetics of skin lesion formation, as overall neutrophil frequency was low at 4 dpi, with no significant difference between wild-type and *Ifnlr1*$^{-/-}$ mice and the increased neutrophil frequency in *Ifnlr1*$^{-/-}$ compared to wild-type mice was first evident during peak disease at 6 dpi and maintained through 8 dpi (Fig. 6B).

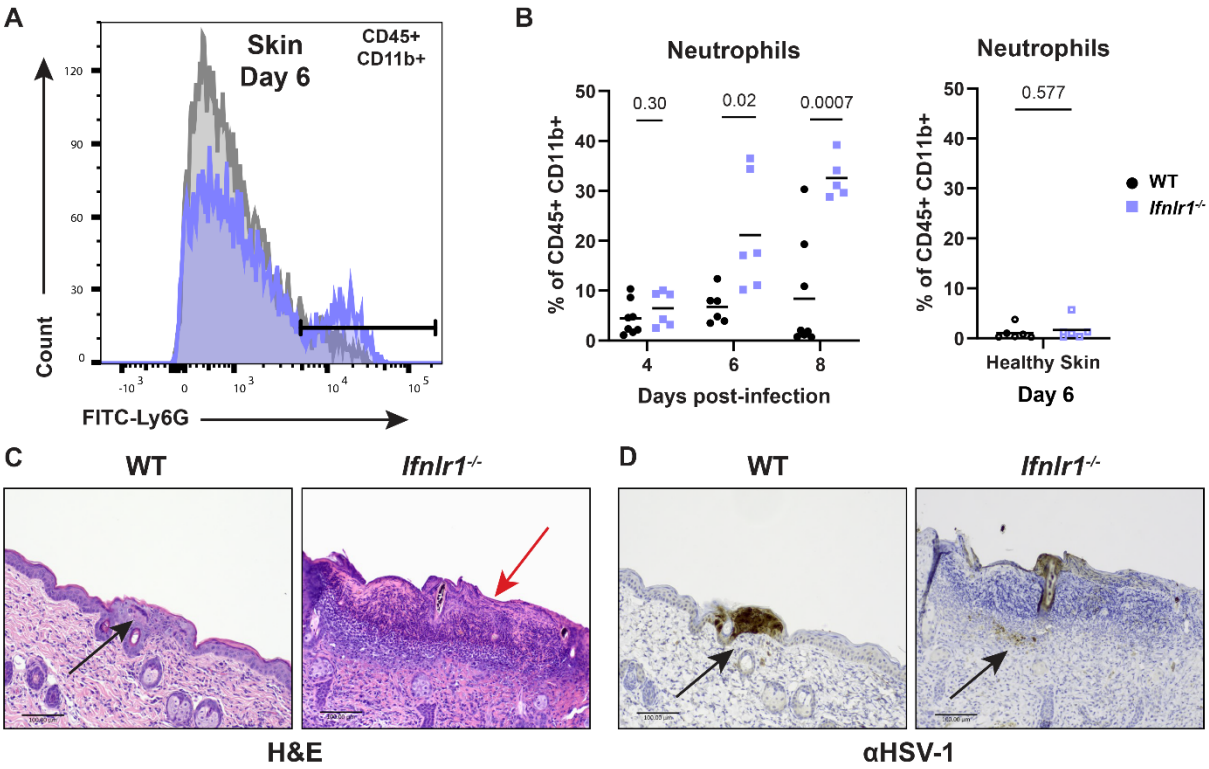

Figure 6. IFN-λ signaling limits neutrophil abundance and severe skin pathology following HSV-1 infection. 8-12 week-old male and female WT and *Ifnlr1*$^{-/-}$ mice were infected with 10^6 FFU of HSV-1. **A-B.** Dermatome lesions and adjacent healthy skin were collected 4-8 dpi and analyzed by flow cytometry. **A.** Representative histogram of WT and *Ifnlr1*$^{-/-}$ lesions showing Ly6G+ neutrophil gating strategy (CD45+, CD11b+, Ly6G+) at 6 dpi. **B.** Frequency of neutrophils (Ly6G+ out of CD45+ CD11b+ live cells) for WT and *Ifnlr1*$^{-/-}$ dermatome lesions and adjacent healthy skin. Significant differences in neutrophil frequency were determined using an unpaired t test. *P* values are reported with $P < 0.05$ considered to be statistically significant. **C-D.** Inoculated flank skin was collected at 6 dpi and serial sections of the same skin lesion were processed for histology. **C.** H&E staining; black arrow denotes a neutrophilic pustule, red arrow denotes diffuse neutrophilic infiltrate. **D.** Anti-HSV-1 immunohistochemistry; viral antigen staining is denoted by black arrows. Scale bars are 100 μm.

To better define the spatial organization of IFN-λ mediated control of neutrophil infiltration, we harvested skin lesions and healthy skin 6 dpi from wild-type and *Ifnlr1*$^{-/-}$ mice and evaluated skin pathology by H&E staining (Fig. 6C) and immunohistochemistry for HSV-1 antigen (Fig. 6D). We found that *Ifnlr1*$^{-/-}$ mice displayed more significant skin damage and overall loss or necrosis of the epidermis in their skin lesions compared to wild-type mice (Fig. 6C, red arrow). In contrast, wild-type mice had a greater number of intact pustules (Fig. 6C, black arrow) compared to *Ifnlr1*$^{-/-}$ mice, which had more diffuse spread of neutrophils throughout the dermis and epidermis. Further, wild-type mice also had an increased staining intensity for HSV-1 antigen compared to *Ifnlr1*$^{-/-}$ mice, in which most staining was evident within pustules (Fig. 6D). HSV-1 antigen was more present in the dermis for *Ifnlr1*$^{-/-}$ mice (black arrows). However, the epidermis was often missing or necrotic in many areas of intense neutrophilic inflammation in *Ifnlr1*$^{-/-}$ mice, possibly precluding antigen detection in the epidermis. Altogether, these data suggest that a lack of IFN-λ signaling results in greater neutrophil infiltration and more severe HSV-1 skin pathology.

IFN-λ signaling suppresses neutrophil-mediated pathology to limit HSV-1 skin disease

To further define the role of neutrophils in driving HSV-1 skin lesion pathology in the absence of IFN-λ signaling, we depleted neutrophils from wild-type and *Ifnlr1*$^{-/-}$ mice 0, 2, and 4 dpi using a αLy6G-depleting antibody (or an isotype-control antibody or PBS) and evaluated dermatome skin lesions 6 dpi (Fig. 7A). To confirm depletion of circulating neutrophils, we collected splenocytes 6 dpi (Fig. 7B) and detected neutrophils (Ly6G+) by flow cytometry. We found that αLy6G antibody efficiently depleted neutrophils compared to isotype-control treated mice (9.8% vs 0.8% Ly6G+ of CD11b+) (Fig. 7B). We found that neutrophil depletion had no effect on skin lesion area in wild-type mice, consistent with prior studies showing that neutrophils do not mediate HSV-1 skin lesion pathology in wild-type mice (Wojtasiak et al., 2010). However, we found that while *Ifnlr1*$^{-/-}$ mice developed significantly larger lesions than wild-type mice and a greater proportion developed severe lesions in mice with intact neutrophils (PBS or isotype-control), IFN-λ-dependent protection was lost in neutrophil-depleted mice (Fig. 7C-D). Altogether

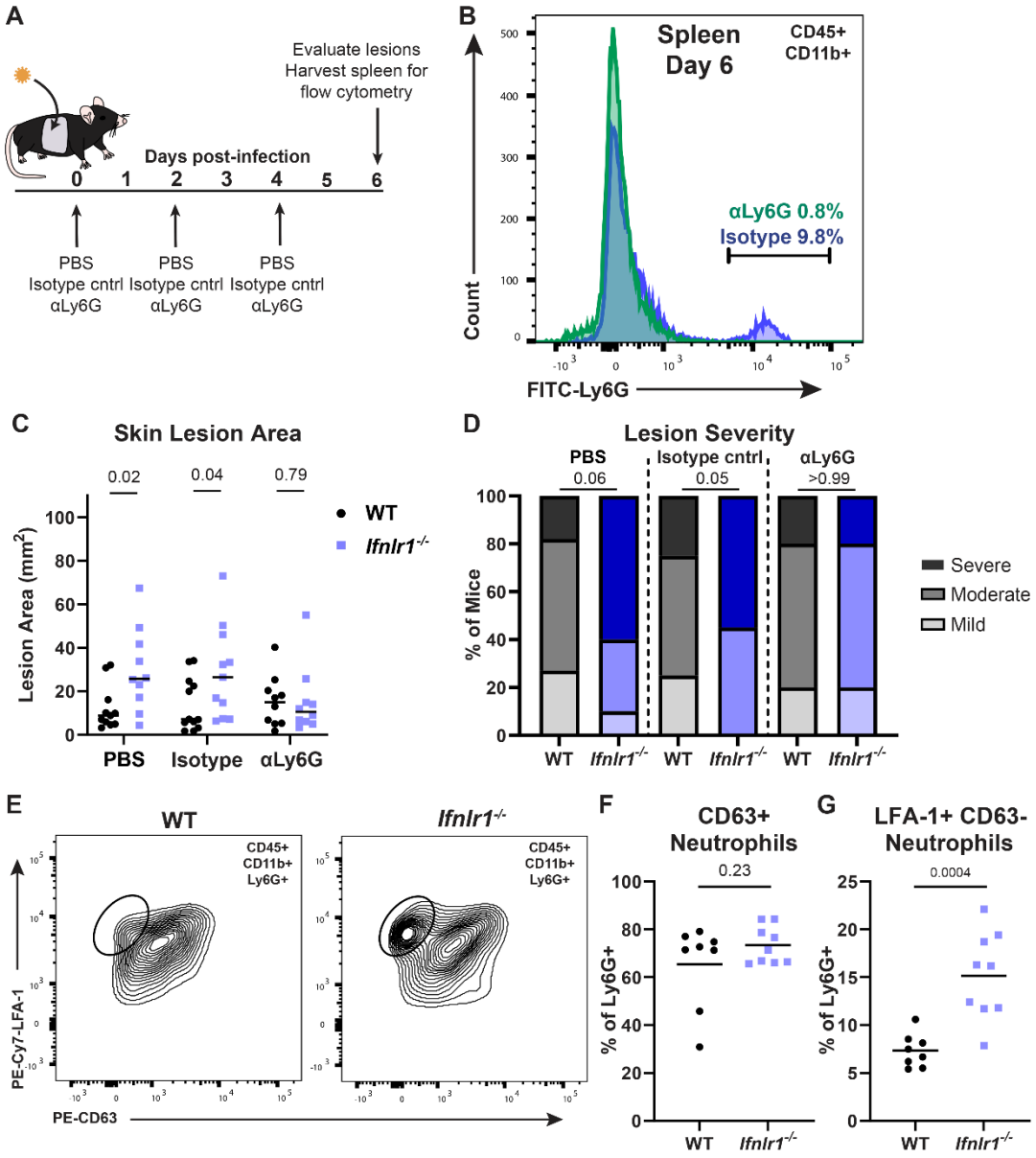

Figure 7. IFN-λ signaling suppresses neutrophil-mediated pathology to limit HSV-1 skin disease. A. Experimental design for neutrophil depletions **B-D.** WT and *Ifnlr1*$^{-/-}$ mice were infected with 10^6 FFU of HSV-1. 0, 2, and 4 dpi mice were injected intraperitoneally with PBS, 250 µg of isotype control (IgG2a), or 250 µg of αLy6G (Clone 1A8). **B.** Spleens were harvested 6 dpi and analyzed by flow cytometry to confirm neutrophil depletion. **C.** Skin lesions were photographed 6 dpi and lesion areas measured ImageJ. **D.** Skin lesion severity was categorized based on 6 dpi lesion area. **E-G.** WT and *Ifnlr1*$^{-/-}$ mice were infected with 10^6 FFU of HSV-1 and 6 dpi skin lesions were photographed and analyzed via flow cytometry. **E.** Representative plots and gating strategy for neutrophil phenotyping markers LFA-1 and CD63 (% of CD45+ CD11b+ Ly6G+). **F.** Frequency of CD63+ neutrophils. **G.** Frequency of LFA-1+ CD63- neutrophils. Differences in lesion area and viral load were compared by Mann-Whitney U test and differences in categorical skin disease were compared by Cochran-Armitage test. Neutrophil frequencies were compared by unpaired t test. *P* values are reported with $P < 0.05$ considered to be statistically significant.

these results suggest that IFN-λ protects against severe HSV-1 skin disease by suppressing neutrophil-driven immunopathology.

To determine the mechanism by which IFN-λ suppresses neutrophil-mediated pathology during HSV-1 skin infection, we investigated whether IFN-λ signaling impacts neutrophil recruitment and/or effector function. We infected wild-type and *Ifnlr1*$^{-/-}$ mice with HSV-1 and collected skin lesions at 6 dpi for flow cytometry. We measured neutrophil expression of lymphocyte function associated antigen 1 (LFA-1, an integrin upregulated upon neutrophil activation and associated with neutrophil recruitment from circulation into inflamed tissues) and CD63 (a lysosomal membrane protein expressed on primary neutrophil granules that is presented on the plasma membrane upon the final stage of neutrophil degranulation) (Fig. 7E-G) (Eichelberger et al., 2019; Phillipson et al., 2006; Zenaro et al., 2015). We found no significant difference in primary granule release (% LFA-1+CD63+) between wild-type and *Ifnlr1*$^{-/-}$ mice (65.4% vs 73.3%, $P > 0.05$) (Fig. 7F). However, we found that skin lesions from *Ifnlr1*$^{-/-}$ mice had a greater proportion of LFA-1+ CD63- neutrophils than wild-type mice, indicative of a population of neutrophils in the skin that are activated and accumulating but have not yet fully degranulated (15.2% vs 7.3%, $P < 0.05$; Fig. 7G). Therefore, our data support a model in which IFN-λ signaling suppresses the accumulation, but not effector functions, of neutrophils in HSV-1 skin lesions, protecting against the development of severe skin pathology.

Neutrophils are known to respond to IFN-λ in the context of other infection and inflammation models in mice (Blazek et al., 2015; Broggi et al., 2017; Espinosa et al., 2017), so we next asked whether the protective effects of IFN-λ against neutrophil-mediated pathology in in the skin required IFN-λ signaling directly in neutrophils. We infected conditional knockout mice lacking IFN-λ signaling in myeloid cells (*LysM*-Cre-*Ifnlr1*$^{-/-}$) or neutrophils (*Mrp8*-Cre-*Ifnlr1*$^{-/-}$) with HSV-1 and evaluated skin lesions and disease severity at 6 dpi, compared to wild-type and *Ifnlr1*$^{-/-}$ mice (Fig. 8A-C). We found that mice that lack IFN-λ signaling exclusively in all myeloid cells or specifically in neutrophils developed skin lesions similar in size to *Ifnlr1*$^{-/-}$ mice (mean area 21.5 mm^2, 19.4 mm^2, and 25.0 mm^2, $P > 0.05$) (Fig. 8B) and with a similar proportion developing severe

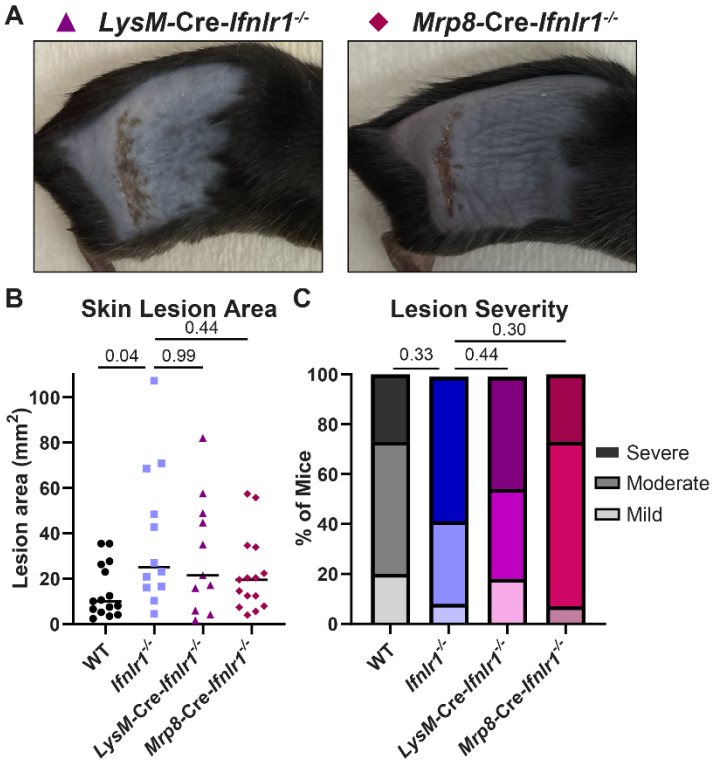

Figure 8. IFN-λ signaling in neutrophils contributes to protection from severe HSV-1 skin disease. 8-12 week-old male and female WT, *Ifnlr1*$^{-/-}$, *LysM*-Cre-*Ifnlr1*$^{-/-}$, and *Mrp8*-Cre-*Ifnlr1*$^{-/-}$ mice were infected with 10^6 FFU of HSV-1. **A.** Dermatome skin lesions were photographed 6 dpi. **B.** Skin lesion areas were measured from photographs 6 dpi using image J. C. Skin lesion severity was categorized based on 6 dpi lesion area. Differences in lesion area and viral load were compared by Mann-Whitney U test. Differences in categorical skin disease were compared by Cochran-Armitage test. *P* values are reported with $P < 0.05$ considered to be statistically significant.

lesions (45%, 27%, 58%, $P > 0.05$) (Fig. 8C). Altogether, these data support a model where IFN-λ signals through keratinocytes and myeloid cells, including neutrophils, to suppress neutrophil accumulation in the skin during HSV-1 infection to control severe HSV-1 skin disease.

IFN-λ signaling in keratinocytes regulates CXCL9 production to restrict neutrophil infiltration and HSV-1 skin pathology

Having established neutrophil recruitment as a key mechanism of IFN-λ-mediated protection against HSV-1 skin disease, we next sought to determine whether the chemokine CXCL9, identified as a DEG in IFN-λ-treated primary keratinocytes (Fig. 5F), mediated neutrophil recruitment in the absence of IFN-λ signaling. Although classically a lymphocyte chemoattractant,

neutrophils also are reported express CXCR3, the receptor for CXCL9, in inflammatory contexts (Boff et al., 2018, 2022; Chami et al., 2014, 2017; Hartl et al., 2008). Furthermore, Forero et al. previously reported that IFN-λ failed to induce expression of *Cxcl9* and other chemokines downstream of a lack of IRF1 induction (Forero et al., 2019). Therefore, we next asked whether IFN-λ acts though keratinocytes via CXCL9 to limit neutrophil infiltration and severe HSV-1 skin disease. First, we measured the concentration of CXCL9 in dermatome lesions and adjacent healthy skin of wild-type and *Ifnlr1*$^{-/-}$ mice 6 dpi (Fig. 9A). We found that *Ifnlr1*$^{-/-}$ mice had significantly higher CXCL9 concentrations in their skin lesions compared to wild-type mice (mean 3191 pg/g vs 1634 pg/g, P = 0.02). The suppressive effect of IFN-λ on CXCL9 was specific to lesioned skin because in adjacent healthy skin CXCL9 concentrations were low and there was no significant difference between wild-type and *Ifnlr1*$^{-/-}$ mice.

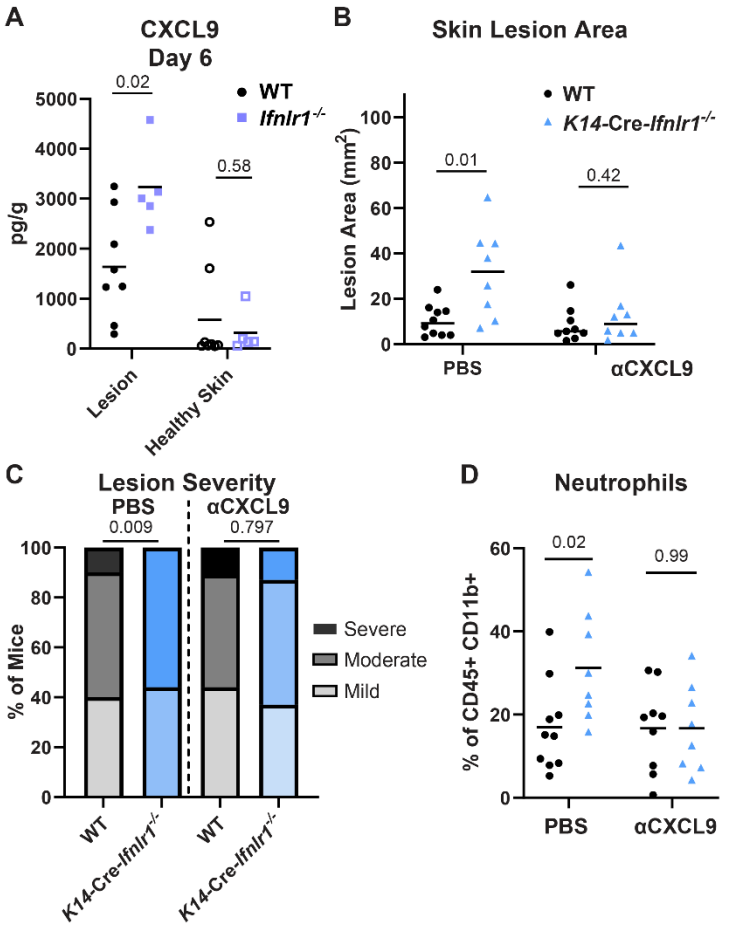

Figure 9. IFN-λ signaling in keratinocytes restricts CXCL9 production to limit neutrophil recruitment and HSV-1 skin disease. 8-12 week-old male and female mice were infected with 10^6 FFU of HSV-1 and skin lesions were analyzed 6 dpi. **A.** CXCL9 was measured by ELISA in homogenates of lesional skin or adjacent healthy skin from WT and *Ifnlr1*$^{-/-}$ mice. **B-D.** WT and *K14*-Cre-*Ifnlr1*$^{-/-}$ mice were infected with HSV-1 and injected intraperitoneally with anti-CXCL9 (300μg) or PBS 0, 2, and 4 dpi. Skin lesion areas were measured from photographs 6 dpi **(B)** and lesion severity categorized **(C)**. **D.** Neutrophil frequency in skin lesions was measured by flow cytometry 6 dpi. Differences in lesion area and viral load were compared by Mann-Whitney U test. Differences in categorical skin disease were compared by Cochran-Armitage test. Differences in CXCL9 concentration and neutrophil frequency were compared by unpaired t test. P values are reported with $P < 0.05$ considered to be statistically significant.

Next, we asked whether CXCL9 contributed to neutrophil recruitment and skin pathology, and whether this occurred downstream of IFN-λ signaling in keratinocytes. We depleted CXCL9 by injecting wild-type

and *K14*-Cre-*Ifnlr1*$^{-/-}$ mice with CXCL9 neutralizing antibody or PBS intraperitoneally 0, 2, and 4 dpi and assessed lesion area, disease severity, and skin neutrophil populations by flow cytometry (Fig. 9B-D). We did not observe any effect of αCXCL9 treatment on lesion area, disease severity, or neutrophil skin infiltration in wild-type mice. Consistent with prior experiments (Fig. 4), we found that PBS-treated *K14*-Cre-*Ifnlr1*$^{-/-}$ mice had larger lesions and more severe disease than wild-type mice (median lesion area 13.0 mm^2 vs 6.7 mm^2, P = 0.01). We also found that *K14*-Cre-*Ifnlr1*$^{-/-}$ mice had significantly greater neutrophil skin infiltration compared to wild-type mice (mean neutrophil frequency 31.3% vs 16.9%, P = 0.02). Strikingly, neutralizing CXCL9 ablated these differences, with *K14*-Cre-*Ifnlr1*$^{-/-}$ mice exhibiting similar lesion areas, disease severity, and neutrophil infiltration compared to wild-type mice after αCXCL9 treatment (Fig.9B-D). Altogether, these data suggest that IFN-λ regulates CXCL9 production in keratinocytes which restricts neutrophil skin infiltration and severe HSV-1 skin disease.

Overall, we report a new protective role for IFN-λ signaling against HSV-1 skin infection. We found that IFN-λ signaling in both keratinocytes and neutrophils is necessary to mediate protection from severe HSV-1 skin disease. We uncovered a mechanism by which IFN-λ signaling in keratinocytes suppresses CXCL9 production to control neutrophil-mediated pathology by limiting neutrophil recruitment and retention in the skin. This is the first report of a protective role for IFN-λ signaling in the skin against an infection and suggests future opportunities for therapeutic uses of IFN-λ against HSV-1 and other skin pathogens.

DISCUSSION

IFN-λ elicits antiviral immunity and maintains barrier integrity at epithelial surfaces, controlling infections locally without the inflammatory immune pathology triggered by the more potent systemic IFN-αβ response (Lazear et al., 2019). Although IFN-λ induces an antiviral transcriptional program most potently in epithelial cells, IFN-λ signaling in leukocytes, such as neutrophils and dendritic cells (DCs), is key to the ability of IFN-λ to induce a protective response

without damaging inflammation (Broggi et al., 2017; Espinosa et al., 2017; Galani et al., 2017; Hemann et al., 2019). Despite the well-established role for IFN-λ in antiviral immunity at anatomic barriers (Lazear et al., 2019), including the respiratory and gastrointestinal tracts (Grau et al., 2020; Peterson et al., 2019; Ye et al., 2019), the blood-brain barrier (Douam et al., 2017; Lazear et al., 2015), and the maternal-fetal interface (Casazza et al., 2022; Jagger et al., 2017), the effects of IFN-λ in the skin have not been extensively investigated. To investigate the role of IFN-λ signaling in the skin, we used HSV-1, an important human pathogen that targets epithelial surfaces including the skin, and which has a well-established mouse model for skin infection (Simmons & Nash, 1984; van Lint et al., 2004; Wang et al., 2019). We found that mice lacking IFN-λ signaling (*Ifnlr1*$^{-/-}$, *Ifnl2/3*$^{-/-}$, or *Ifnar1*$^{-/-}$ *Ifnlr1*$^{-/-}$) developed larger HSV-1 skin lesions compared to their IFN-λ sufficient counterparts. However, lesion size was uncoupled from skin viral loads, suggesting a role for IFN-λ in suppressing inflammatory immune pathology during HSV-1 skin infection. Using conditional knockout mice, we found that IFN-λ signaling in both keratinocytes and leukocytes was necessary for protection from severe skin disease. We further showed that neutrophils are required for the enhanced skin pathology observed in *Ifnlr1*$^{-/-}$ mice and that IFN-λ signaling in neutrophils contributes to the protective effect of IFN-λ against HSV-1 skin disease. Altogether, our results support a model where IFN-λ exerts an immunomodulatory role during HSV-1 skin infection, suppressing neutrophil-mediated pathology.

IFN-λ suppresses neutrophil recruitment and pathology in colitis and rheumatoid arthritis models (Blazek et al., 2015; Broggi et al., 2017), as well as during influenza virus infection (Galani et al., 2017). Our results add to a growing number of systems that demonstrate a role for neutrophils as a key IFN-λ responsive cell type in mice and broaden the range of mechanisms by which IFN-λ impacts neutrophil function, although there is still debate regarding the extent to which human neutrophils respond to IFN-λ (Broggi et al., 2017; Espinosa et al., 2017; Goel et al., 2020; Santer et al., 2020). Neutrophils are recruited to the skin during HSV-1 skin infection but are not important for mediating skin pathology in wild-type mice (Hor et al., 2017; Wojtasiak et al.,

2010). Our studies revealed a pathogenic role for neutrophils during HSV-1 skin infection but only in the absence of IFN-λ signaling, identifying a key role for IFN-λ in suppressing the pathogenic activity of neutrophils that are recruited into the skin during HSV-1 infection.

While our studies first focused on the protective effects of IFN-λ signaling in leukocytes, specifically neutrophils, we found that IFN-λ signaling in keratinocytes also was required to restrict HSV-1 skin disease. To investigate the mechanism by which IFN-λ signaling in keratinocytes modulates skin immunity to control HSV-1 skin disease, we performed bulk RNA-seq analysis in primary mouse keratinocytes, as well as in a human epithelial cell line (A549). Our data from A549 cells supports the standard paradigm that the transcriptional response induced by IFN-λ is less potent than the IFN-β response. However, in primary keratinocytes we found that many ISGs were induced equivalently by IFN-λ and IFN-β. These observations are consistent with other transcriptional profiling experiments in primary cells (Caine et al., 2019; Galani et al., 2017) suggesting that experiments in cell lines may underestimate the potency of the IFN-λ response. A notable difference between the IFN-λ and IFN-β responses in keratinocytes was the chemokine CXCL9, which was only weakly induced by IFN-λ compared to IFN-β, consistent with prior work showing that IFN-λ failed to induce expression of CXCL9 and other chemokines, downstream of a lack of STAT1 homodimer formation and IRF1 induction (Forero et al., 2019). Although we found that the IFN-β response was not impacted by the lack of IFN-λ signaling, the IFN-λ response was diminished in both keratinocytes and A549 cells lacking IFN-αβ signaling, suggesting a possible role for cross-talk between the IFN-λ and IFN-αβ responses.

While we found greater accumulation of neutrophils in skin lesions from *Ifnlr1*$^{-/-}$ mice compared to wild-type mice and showed that neutrophils were necessary for the severe skin pathology observed in *Ifnlr1*$^{-/-}$ mice, the mechanism by which IFN-λ modulates neutrophil function to protect against HSV-1 skin disease remains unclear. We found no difference in CD63 expression in neutrophils from *Ifnlr1*$^{-/-}$ mice compared to wild-type mice, suggesting that IFN-λ does not act to inhibit degranulation in this system. We did find that *Ifnlr1*$^{-/-}$ mice exhibited

increased expression of the lectin LFA-1, which promotes tissue recruitment and retention of neutrophils, consistent with a model where IFN-λ signaling reduces neutrophil retention in HSV-1 skin lesions. Accordingly, *Cxcl9* was among the genes with reduced induction by IFN-λ compared to IFN-β in primary keratinocytes, CXCL9 levels in skin lesions were higher in the absence of IFN-λ signaling, and depleting CXCL9 ablated the enhanced neutrophil infiltration and large skin lesion phenotypes of *K14*-Cre-*Ifnlr1*$^{-/-}$ mice. Altogether these data support a model where in the absence of IFN-λ signaling, keratinocytes overproduce CXCL9, stimulating excessive neutrophil infiltration and retention into HSV-1 infected skin, exacerbating skin disease severity.

In addition to HSV-1, we also found a protective role for IFN-λ in HSV-2 skin infection. Like HSV-1, HSV-2 produced larger skin lesions in the absence of IFN-λ signaling, although the average severity of HSV-2 lesions was greater than HSV-1 and the kinetics of the infection were slower. The fact that we observed a similar role for IFN-λ for both HSV-1 and HSV-2 supports a general role for IFN-λ in controlling viral skin infections; future studies will investigate the protective effects of IFN-λ against other viral pathogens that target the skin, including poxviruses, papillomaviruses, and arboviruses, as well as bacterial, fungal, and protozoan skin pathogens. We also evaluated whether IFN-λ protected against HSV vaginal infection, since the vaginal epithelium is a plausible site for IFN-λ activity and IFN-λ has been reported to protect against vaginal HSV-2 and Zika virus infections (Ank et al., 2008; Caine et al., 2019). HSV-1 vaginal infection typically does not produce overt disease in mice, whereas HSV-2 produces disease signs that can be evaluated in addition to measuring viral loads. Prior work with HSV-2 vaginal infection in wild-type mice showed that neutrophil recruitment to the vagina worsened disease severity (Lebratti et al., 2021), further supporting the premise for a protective role for IFN-λ at this epithelial barrier. However, we found no difference in overt vaginal disease in *Ifnlr1*$^{-/-}$ mice compared to wild-type mice infected with HSV-2. These results are consistent with our previous observations with Zika virus, where we found no difference in vaginal wash viral loads from *Ifnlr1*$^{-}$

526 $^{/-}$ mice compared to wild-type mice (Lopez et al., 2022). Additionally, our data are consistent with
527 other reports for Zika virus and HSV-2 vaginal infections, as these experiments only found
528 protective effects for IFN-λ signaling when pretreating mice intravaginally with recombinant IFN-
529 λ or Toll-like receptor 3 (TLR-3) or TLR-9 agonists (Ank et al., 2008; Caine et al., 2019), as
530 opposed to evaluating phenotypes in *Ifnlr1*$^{-/-}$ mice. Overall, these observations suggest any
531 protective effect of IFN-λ in the vagina may be context-dependent and likely does not serve to
532 restrict viral replication. The difference in phenotypes for IFN-λ signaling against HSV-2 infection
533 in the skin and the vagina also underscores possible differences in mechanisms of immunity at
534 these different epithelial barriers.

535 Although our work has focused on IFN-λ-mediated protection from HSV-1 in context of
536 healthy skin, it will be interesting to evaluate these effects in the context of dermatological
537 conditions such as atopic dermatitis (also called eczema). Patients with atopic dermatitis are
538 susceptible to severe HSV-1 skin infections (eczema herpeticum) (Wollenberg et al., 2003).
539 Notably, atopic dermatitis skin lesions exhibit diminished IFN-λ production compared to healthy
540 skin from the same patients (Wolk et al., 2013) and injection of recombinant IFN-λ reduced the
541 severity of eczema herpeticum in mice (Kawakami et al., 2017). Atopic dermatitis patients also
542 are susceptible to severe infections by poxviruses, posing a hazard to individuals who require
543 smallpox vaccination (due to risk of exposure to or laboratory work with variola virus, vaccinia
544 virus, or other orthopoxviruses) (Reed et al., 2012; Wharton et al., 2003). We expect that the
545 mechanisms by which IFN-λ restricts HSV-1 skin disease will be relevant to other skin infections,
546 particularly where pathogen-triggered immune pathology produces skin lesions, such as vaccinia
547 virus and *Leishmania* (Novais et al., 2021; Shmeleva et al., 2022).

548 We found that *Ifnlr1*$^{-/-}$ mice developed larger HSV-1 skin lesions compared to wild-type
549 mice, even though there was no difference in viral loads in the skin, supporting an
550 immunomodulatory, rather than antiviral, role for IFN-λ in the skin. However, in this system, IFN-
551 λ is induced in the skin in response to HSV-1 infection, meaning that the virus has a head start

and can employ its arsenal of strategies to antagonize the host IFN response. When we instead pre-treated mice with topical IFN-λ prior to infection, we found lower viral loads in IFN-λ treated mice compared to PBS-treated mice, indicating that IFN-λ can have an antiviral effect against HSV-1 in the skin. IFN-λ has demonstrated therapeutic utility against a variety of viral infections, including hepatitis C virus, hepatitis B virus, and SARS-CoV-2 in human studies, as it is thought to confer protective antiviral activity without the damaging immune pathology induced by IFN-αβ treatment (Feld et al., 2021; Lazear et al., 2019). The skin is an especially attractive site to leverage the protective effects of IFN-λ, due to its easy accessibility for topical administration. Encouragingly, topical IFN-λ treatment restricted HSV-1 corneal infection in mice (Miner et al., 2020). Future studies will investigate the potential for topical IFN-λ treatment as a therapy for HSV and other skin infections.

Altogether, our data provide the first evidence of a skin-specific role for IFN-λ in controlling a viral infection. We detail a mechanism by which IFN-λ signals through both keratinocytes and leukocytes to limit severe HSV-1 skin disease. We found that IFN-λ signaling suppresses neutrophil recruitment to the skin, in part by suppressing CXCL9, and the excess recruitment of neutrophils to the skin in the absence of IFN-λ signaling is the driver of pathology. This keratinocyte-neutrophil axis via CXCL9 provides new insights into the immunomodulatory effects of IFN-λ at barrier sites, including the skin.

MATERIALS AND METHODS

Viruses and Cells Virus stocks were grown in Vero (African green monkey kidney epithelial) cells. Vero and A549 (ATCC# CCL-185) cells were maintained in Dulbecco's modified Eagle medium (DMEM) containing 5% heat-inactivated fetal bovine serum (FBS) and L-glutamine at 37°C with 5% CO2. Virus stocks were grown in DMEM containing 2% FBS, L-glutamine, and HEPES at 37°C with 5% CO_2. HSV-1 strain NS was obtained from Dr. Harvey Friedman (University of Pennsylvania) (Friedman et al., 1981). HSV-2 strain 333 was obtained from Dr.

578 Steven Bachenheimer (UNC). Virus stock titers were determined by focus-forming assay on Vero
579 cells. Viral foci were detected using 1:10,000 dilution of αHSV rabbit antibody (Dako) and 1:50,000
580 dilution of goat αrabbit HRP conjugated antibody, and TrueBlue peroxidase substrate (KPL).
581 Antibody incubations were performed for at least 1 hour at room temperature. Foci were counted
582 on a CTL Immunospot analyzer.

583 **Mice** All experiments and husbandry were performed under the approval of the University of
584 North Carolina at Chapel Hill Institutional Animal Care and Use Committee. Experiments used 8-
585 12-week-old male and female mice on a C57BL/6 background. Wild-type mice used in Figure 3
586 and S1 were purchased from Jackson Labs and then bred in house. *Ifnlr1*$^{-/-}$ mice were generated
587 by two breeding schemes. For *Ifnlr1*$^{-/-}$ mice in Figures 1, 5, 6, and 7 mice were generated by
588 crossing *Ifnlr1*$^{f/f}$ mice with mice expressing Cre recombinase under control of an Actin promoter.
589 These mice were bred as Cre hemizygotes to generate mixed litters in which 50% of mice retained
590 IFN-λ signaling and 50% lacked IFN-λ signaling. For *Ifnlr1*$^{-/-}$ mice in Figure 4 and 8, mice were
591 generated by crossing *Ifnlr1*$^{f/f}$ mice with mice expressing Cre recombinase under control of an
592 CMV promoter. After generation, mice were bred as Cre homozygote knockout by knockouts and
593 experimental *Ifnlr1*$^{-/-}$ mice were genotyped periodically to verify *Ifnlr1* knockout status. *K14*-Cre-
594 *Ifnlr1*$^{-/-}$, *Vav*-Cre-*Ifnlr1*$^{-/-}$, *LysM*-Cre-*Ifnlr1*$^{-/-}$, and *Mrp8*-Cre-*Ifnlr1*$^{-/-}$ mice were generated by crossing
595 *Ifnlr1*$^{f/f}$ mice with mice expressing Cre recombinase under control of a *Vav* promoter (Jackson
596 Labs #8610), a *K14* promoter (obtained from Dr. Scott Williams, UNC), a LysM promoter (Jackson
597 Labs #4781, obtained from Dr. Jenny Ting, UNC), or a *Mrp8* promoter (Jackson Labs #21614),
598 respectively. Mice were bred as Cre hemizygotes to generate mixed litters in which 50% of mice
599 retained IFN-λ signaling and 50% lacked IFN-λ signaling in specific cell types. After data analysis,
600 experimental mice were genotyped by PCR on tails for both Cre and *Ifnlr1* status. *Ifnar1*$^{-/-}$ mice
601 were obtained from Dr. Jason Whitmire (UNC) then bred in-house. *Ifnar1*$^{-/-}$ *Ifnlr1*$^{-/-}$ DKO mice were
602 generated by crossing *CMV*-Cre *Ifnlr1*$^{-/-}$ and *Ifnar1*$^{-/-}$ mice and bred in house. *Ifnl2/3*$^{-/-}$ mice were
603 obtained from Dr. Megan Baldridge (Washington University in St. Louis) and then bred in house.

Ifnk$^{-/-}$ mice were generated in the laboratory of Dr. Michael Diamond (Washington University in St. Louis). Embryonic stem (ES) cells (C57BL/6 background) were obtained from the knockout mouse project (KOMP). The ES cells contained a LacZ reporter-tagged deletion allele with a neomycin selection cassette (Ifnk$^{tm1(KOMP)Vlcg}$). Mice derived from these ES cells were crossed to mice expressing Cre recombinase under a CMV promoter to excise the neomycin selection cassette. The resulting *Ifnk*$^{-/-}$ mice were bred at UNC for use in experiments. Genetic background was confirmed by miniMUGA genotyping array.

HSV Skin Infections One day prior to infection, mice were anesthetized by nose-cone isoflurane and depilated manually by plucking the fur from the right flank. One day later, mice were anesthetized by chamber isoflurane for infections. To perform infections, we abraded the skin of anesthetized, depilated mice with ~10x closely spaced punctures (over ~5 mm^2) using a Quintip skin test allergy needle. Immediately after abrasion, we overlaid 10 µL of viral inoculum (virus + 1% FBS in PBS) and allowed the inoculum to dry while mice were anesthetized.

PCR Genotyping *Ifnlr1*, *Cre*, *Ifnl2/3,* and *Ifnk* genotypes were determined by PCR on tail samples (unless otherwise indicated) on DNA extracted using the Quantabio supermix and the following previously described primers:

Ifnlr1 $F_1$5-AGGGAAGCCAAGGGGATGGC-3′, $R_1$5′-AGTGCCTGCTGAGGACCAGGA-3′, $R_2$5′-GGCTCTGGACCTACGCGCTG-3′;

Cre $F_1$5′-CGTACTGACGGTGGGAGAAT-3′, $R_1$5′-CCCGGCAAAACAGGTAGTTA-3′;

Ifnl2/3 F_{KO}5′-CACACTGTGGACAGGCCAT-3′, R_{KO}5′-ACCAGCCTGAGGTCCCTAGT-3′, F_{WT}5-TGGAGTCCAGAGCAGCTTTT-3′, R_{WT}5′-TCCACCCAGAAGCAAAGAAC-3′;

Ifnk $F_1$5′-CCTGTGTGTCAGGTTTAC-3′, $R_1$5′-TGCCCAACTCCAGGTAGAC-3′, $R_2$5′-GTCTGTCCTAGCTTCCTCACTG -3′;

K14-Cre (used for colony establishment) $F_1$5′- CACGATACACCTGACTAGCTGGGTG-3′, $R_1$5′-CATCACCCACAGGCTAGCGCCAACT-3′;

Vav-Cre (used for breeders) $F_1$5′- AGATGCCAGGACATCAGGAACCTG-3′, $R_1$5′-ATCAGCCACACCAGACACAGAGATC-3′.

Focus-forming Assay Viral loads were measured by focus-forming assay in which tissues were weighed, homogenized using beads and DMEM with 2% FBS and 1% HEPES and serially diluted in a round bottom 96-well plate. 100 µL of each dilution was then transferred to monolayers of Vero cells (96 well plate with $2x10^4$ cells/well plated 1 day prior) in duplicate and incubated at 37°C for 1 hour. Thereafter, wells were overlaid with 125 µL methylcellulose (1% methylcellulose in 1X MEM+ 2% FBS, L-Glut, P/S, HEPES) and left to incubate at 37 °C for 20h. After 20h, plates were fixed by adding 4% paraformaldehyde (PFA) 100 µL/well for 60 min at room. After fixing, PFA and overlay was flicked off and the plates were washed 3x with PBS+1%Tween using a handheld plate washer. Foci were detected using 1:10,000 dilution of αHSV rabbit antibody (Dako) and 1:50000 dilution of goat αrabbit HRP conjugated antibody, and TrueBlue peroxidase substrate (KPL). Antibody incubations were performed for at least 1 hour at 24°C. Foci were counted on a CTL Immunospot analyzer.

Viral Genome Quantification by qPCR Viral genomes were quantified from pooled DRG samples (L2-L5 from the ipsilateral or contralateral sides) that were homogenized in 500 µL of PBS and beads. DNA was extracted from 200 µL of homogenate using the Qiagen DNeasy Blood & Tissue Kit (#69504). HSV-1 DNA was quantified by TaqMan qPCR on a CFX96 Touch real-time PCR detection system (Bio-Rad) against a standard curve generated by extracting DNA from an HSV-1 viral stock. HSV-1 genomes were detected using the following primers targeting the U_L23 gene: F primer 5′-TTGTCTCCTTCCGTGTTTCAGTT-3′, R primer 5′-GGCTCCATACCGACGATCTG-3′, and probe 5′-FAM-CCATCTCCCGGGCAAACGTGC-MGB-NFQ-3′ (Ma et al., 2014).

Lesion Area Quantification and Categorization To measure HSV lesion areas, mice were anesthetized and photographed using an iPhone camera next to a ruler and an identifying card. Thereafter, images were analyzed using ImageJ in which pixels were converted to millimeters

using the reference ruler and then lesions were outlined using the freehand tool and calculated area within the freehand designations were reported. Lesions analyzed 6 dpi were categorized using the following system: <5 mm^2 = Mild, 5-23 mm^2 = Moderate, and >23 mm^2 = Severe.

HSV-2 Vaginal Infections and Disease Categorization To infect mice with HSV-2 vaginally, experimental mice were treated 5 days prior with 2 mg DepoProvera (UNC Pharmacy) via subcutaneous inoculation. On the day of infection, mice were inoculated with 10^3 FFU/10µL of HSV-2 strain 333 intravaginally. Mice were monitored for disease signs starting 4 dpi and categorized using the following scoring system (Lebratti et al., 2021): 0: no inflammation, 1: mild redness and swelling, 2: visible ulceration and fur loss, 3: severe ulceration and signs of sickness, 4: hindlimb paralysis, 5: moribund/dead.

Bone Marrow Chimeras Bone marrow chimera mice were generated by lethally irradiating wild-type and *Ifnl2/3*$^{-/-}$ mice (2x600 CGy) and injecting 10^7 bone marrow cells from complementary and reciprocal donors. After irradiation, mice were given sulfamethoxazole (6 mg/ml) in their drinking water for the duration of their life. Mice were infected with HSV-1 and photographed and harvested 6 dpi. Efficient bone marrow transfer was validated at the end of the experiment by PCR genotyping tail, ear skin, and whole blood from each mouse for *Ifnl2/3*.

Flow Cytometry For analysis by flow cytometry, tissues were harvested into cold DMEM + 10% FBS and processed using established methods for digestion of whole mouse back skin (Lou et al., 2020). In brief, samples were cut into thirds and incubated overnight at 4°C in 5 mg/mL Dispase II (Sigma) in Hanks Buffered Salt Solution (HBSS). Afterwards, samples were washed 1x with cold PBS and epidermis and dermis were mechanically separated for separate enzymatic digestions. The epidermis was digested in 1 mL 0.05% trypsin (Fisher) for 30 min at 37°C. Separately, the dermis was digested in 3 mL dermal dissociation solution (1 mg/mL Collagenase P (Sigma), 100 µg/mL DNAse I (Fisher) for 1 hour at 37°C. After incubation, matched epidermal and dermal digestions were combined and passed through a 70µm cell strainer and resuspended

in DMEM + 10% FBS. Suspensions were then centrifuged at 400xg for 5 min at 4°C and resuspended in PBS + 1% FBS (staining buffer) and stained with fluorescent antibodies.

Fc Block and all fluorescent antibodies were sourced from Biolegend and titrated prior to use. Samples were treated with Fc Block for 10 min at 4°C prior to staining. Afterward, samples were washed 3x in staining buffer and then stained for cell surface antigens for 20 min at 4°C. Cells were then washed 3x, fixed with 2% paraformaldehyde solution and analyzed on an LSRII (BD). Data were analyzed with FlowJo software (v10.8). The following fluorescent antibodies (and specific clones) were used: αCD3 (145-2C11), αEPCAM (G8.8), αCD8a (54-6.7), αCD4 (CK1.5), αCD45 (30-F11), αNK1.1 (PK136), αLy6G (IA8), αCD11c (N418), Fc Block αCD16/32 (93), αCD11b (M1/70), αCD19 (6D5), αLy6C (HK1.4) αCD63 (NVG-2), αLFA-1 (H155-78), Zombie UV Fixable Dye. Gating strategies for neutrophils are shown in Fig. S3. All gating strategies for all cell types and neutrophil phenotyping markers were based upon published immunophenotyping methods (Eichelberger et al., 2019; Lou et al., 2020; Sakamoto et al., 2021).

Histopathology Samples were prepared for histology by collecting the entire depilated region of the right flank (lesional and healthy skin), flattening the skin on cardstock, and submerging in 10% Neutral Buffered Formalin for 48 hr at 4°C. After fixation, skins were washed and resuspended in 70% ethanol and stored at 4°C until submission to the UNC Pathology Services Core Facility. To prepare fixed skin for submission, two cuts of skin were taken: 1) a horizontal section through the flank to capture lesion and healthy skin and 2) a vertical cut to capture the diseased dermatome region of skin. Thereafter, samples were stored in 70% ethanol and processed by the core, stained for H&E and HSV-1 (1:1000, Dako), and analyzed by a veterinary pathologist (Dr. Hannah Atkins), who selected representative images and identified regions of interest.

Neutrophil and CXCL9 Depletions To deplete neutrophils, mice were injected intraperitoneally 0, 2, and 4 dpi with 250µg in 200µL of αLy6G antibody (Clone 1A8 IgG2a, BioXCell) or with isotype control antibody (BioXCell) or PBS. Systemic depletion of neutrophils was validated at the end of the experiment in each cohort of mice using the gating strategy outlined in supplementary Fig. 3B

on splenocytes. To neutralize CXCL9, mice were injected intraperitoneally 0, 2, 4 dpi with 300 µg in 200 µL of αCXCL9 antibody (Clone MIG-2F5.5 IgG, BioXCell).

CXCL9 ELISA To measure the concentration of CXCL9 in the skin, lesional and healthy skin were collected from wild-type and *Ifnlr1*$^{-/-}$ mice 6 dpi. Samples were weighed and then homogenized using beads and resuspended in 1 mL of DMEM. CXCL9 was measured from homogenized skin supernatants using the MIG/CXCL9 Mouse ELISA Kit (ThermoFisher, #EMCXCL9) using optical density read at 450nm and fit against the standard curve according to manufacturer protocol.

IFN-λ Topical Pre-treatment To prophylactically treat mice with IFN-λ, mice were depilated by plucking 2 days prior to infection. The next day, 5 µg of recombinant murine IFN-λ3 (PBL #12820) in 10 µL PBS (or PBS alone) was applied topically to a 5mm^2 region of skin and allowed to air dry. The treated area of skin was circled with a Sharpie and 24 hours later mice were infected with HSV-1 at the treated site.

Generating IFN Receptor Knockout A549 Cell Lines IFN receptor knockout cell lines were generated in an A549 background using CRISPR/Cas9 gene editing. A single guide RNA targeting exon 2 of IFNAR1 (5'-CACCGTAGATGACAACTTTATCCTG-3'), exon 3 of IFNLR1 (5'-CACCGACAAGTTCAAGGGACGCGTG-3'), and a non-targeting control (5'-CACCGGTATAATACACCGCGCTAC-3') were cloned into the lentiCRISPRv2 vector (Addgene). The gRNA construct was then co-transfected with two packaging plasmids (pMD2.G and pSPAX2, Addgene) into HEK293T cells to produce lentiviruses. A549 cells were transduced and selected using 2.5 µg/ml puromycin for two weeks. Surviving cells were then single cell sorted into 96 well plates using a FACS ARIA II flow cytometer. Single clones of knockout monoclonal cultures were confirmed via Sanger sequencing and used for subsequent experiments.

Primary Mouse Keratinocyte Isolation Keratinocytes were isolated from adult male and female mice of indicated genotypes using published protocols (Li et al., 2017). In brief, mice were euthanized and whole tails were harvested into cold PBS. Tail skin was peeled off, cut into thirds, and digested overnight at 4^{o}C in 4 mg/mL Dispase II (Sigma) while rotating. The epidermis was

then mechanically peeled from the dermis and placed basal side down into 0.05% trypsin to shake for 20 min at room temperature. Afterwards, 7 mL of DMEM with 10% FBS was added and the epidermis was rubbed basal side down into the bottom of a petri dish to release basal keratinocytes. Cell suspensions were collected, passed through a 70 µm cell strainer, and pelleted at 400xg for 5 min. Cell pellets were resuspended in DermaLife K Keratinocyte Medium without antibiotics (Lifeline, Cat #LL-007) to $1x10^5$ cells/mL and seeded 1mL/well in 12-well plates. One adult mouse tail generally yields ~$1x10^5$ cells. Keratinocytes were grown to confluence, ~3-4 days, with media changes every other day, prior to experimental use.

IFN treatments in Cell Culture Primary mouse keratinocytes in 12-well plates were grown to confluence for 3-4 days after isolation. Recombinant murine IFN-β (5 ng/mL; PBL #12401) or IFN-λ3 (5 ng/mL; PBL# 12820) was resuspended in fresh keratinocyte growth media and 1 mL of IFN suspension or media alone was added to cells. 24 hours later, supernatant was removed, 350 µL of Buffer RLT (Qiagen) was added to each well, and samples were stored at -80 °C until RNA extraction. A549 cells were treated similarly at confluence in 6-well plates with recombinant human IFN-β (5 ng/mL; PBL #11415) or IFN-λ2 (50 ng/mL; PBL #11720) or media only, resuspended in A549 growth media. Then, 8 hours later, supernatant was removed, 350 µL of Buffer RLT (Qiagen) was added to each well, and samples were stored at -80°C until RNA extraction.

RNA extractions and qRT-PCR RNA from primary keratinocytes and A549 cells was extracted with the Qiagen RNAeasy minikit. Predesigned primer/probe sets (Integrated DNA Technologies) were used to detect murine *Ifit1* (Mm.PT.58.32674307) and *ActB* (Mm.PT.39a.22214843.g) and human *IFIT1* (Hs.PT.56a.20769090.g) and *ACTB* (Hs.PT.39a.22214847). Transcripts were measured by TaqMan one-step qRT-PCR on a CFX96 Touch real-time PCR detection system (Bio-Rad) and were reported as relative differences in threshold cycle (Ct) values between ISG and actin as a housekeeping gene using the $2^{-\Delta\Delta Ct}$ with reference to the average of media-treated, wild-type primary keratinocytes or RenLuc A549s for each sample.

RNA Sequencing RNA extracted from A549 cells and primary keratinocytes with the indicated IFN treatments was prepared for RNA sequencing by the UNC High Throughput Sequencing Facility using the Kapa mRNA stranded library prep kit. Primary keratinocytes were sequenced using NovaSeq6000S4 XP Paired End 2x100 and A549 cells were sequenced using NovaSeq6000S4 XP Paired End 2x150. Sequences were analyzed using CLC Genomics Workbench version 23.0.4 (Qiagen) with references to *Mus musculus* reference genome sequence and annotation mm10 (Ensembl GRCm39.110) and *Homo sapiens* reference genome sequence and annotation hg38 (Ensembl GRCh38. 110) for sequences from primary keratinocytes and A549 cells, respectively, using default settings. Gene lists were then analyzed using principal component analysis and volcano plot tools within CLC Genomics Workbench. Differentially expressed genes were defined by having a false discovery rate (FDR) < 0.05 and an absolute value Log_2 Fold Change > 1. Statistics were calculated within CLC Genomics Workbench and volcano plots were prepared for visualization using Graphpad Prism 9 and principal component analysis plots using CLC Genomics Workbench. Raw and processed RNA sequencing data is available under the GEO superseries accession number GSE242171.

Statistics All statistics (apart from RNAseq data) were calculated using GraphPad Prism 9 or XLSTAT 2022 Plugin. Lesion area, viral loads, and vaginal disease score were analyzed using a Mann-Whitney U test and adjusting for multiple comparisons using the Holm-Šídák method when appropriate. Flow cytometry was analyzed using an unpaired t-test. HSV-1 skin disease severity was analyzed using the Cochrane-Armitage Method and adjusting for multiple-comparisons using the Benjamini and Hochberg method when appropriate. Survival curves were analyzed using the Mantel-Cox Log Rank test.

ACKNOWLEDGEMENTS

This work was supported by R01 AI139512 and R01 AI175708 (H.M.L.). D.T.P. was supported by T32 AI007419 and F31 AI167502. IM and JKW were supported by R01 AI138337, R01

AI131685, R01 AI143894 to JKW, and R21 AI163606 to IM, and a DoD award W81XWH2110919 (JKW). The UNC flow cytometry core facility is supported by a NCI Center Core Support Grant (5P30CA016086). We gratefully acknowledge the technical support from the UNC High Throughput Sequencing Facility. This facility is supported by the University Cancer Research Fund, Comprehensive Cancer Center Core Support grant (P30-CA016086) and the UNC Center for Mental Health and Susceptibility grant (P30-ES010126). The authors have no competing financial interests.

SUPPLEMENTARY MATERIALS

Supplementary Figures 1-4

Supplementary Table 1: RNAseq data from A549 cells

Supplementary Table 2: RNAseq data from primary keratinocytes

REFERENCES

1. Ank, N., Iversen, M. B., Bartholdy, C., Staeheli, P., Hartmann, R., Jensen, U. B., Dagnaes-Hansen, F., Thomsen, A. R., Chen, Z., Haugen, H., Klucher, K., & Paludan, S. R. (2008). An important role for type III interferon (IFN-lambda/IL-28) in TLR-induced antiviral activity. *Journal of Immunology (Baltimore, Md.: 1950)*, *180*(4), 2474–2485. https://doi.org/10.4049/jimmunol.180.4.2474
2. Baldridge, M. T., Lee, S., Brown, J. J., McAllister, N., Urbanek, K., Dermody, T. S., Nice, T. J., & Virgin, H. W. (2017). Expression of Ifnlr1 on Intestinal Epithelial Cells Is Critical to the Antiviral Effects of Interferon Lambda against Norovirus and Reovirus. *Journal of Virology*, *91*(7), e02079-16. https://doi.org/10.1128/JVI.02079-16
3. Blazek, K., Eames, H. L., Weiss, M., Byrne, A. J., Perocheau, D., Pease, J. E., Doyle, S., McCann, F., Williams, R. O., & Udalova, I. A. (2015). IFN-λ resolves inflammation via

809 suppression of neutrophil infiltration and IL-1β production. *The Journal of Experimental*
810 *Medicine*, *212*(6), 845–853. https://doi.org/10.1084/jem.20140995
811 **4.** Boff, D., Crijns, H., Janssens, R., Vanheule, V., Menezes, G. B., Macari, S., Silva, T. A.,
812 Amaral, F. A., & Proost, P. (2018). The chemokine fragment CXCL9(74-103) diminishes
813 neutrophil recruitment and joint inflammation in antigen-induced arthritis. *Journal of*
814 *Leukocyte Biology*, *104*(2), 413–422. https://doi.org/10.1002/JLB.3MA1217-502R
815 **5.** Boff, D., Russo, R. C., Crijns, H., de Oliveira, V. L. S., Mattos, M. S., Marques, P. E.,
816 Menezes, G. B., Vieira, A. T., Teixeira, M. M., Proost, P., & Amaral, F. A. (2022). The
817 Therapeutic Treatment with the GAG-Binding Chemokine Fragment CXCL9(74-103)
818 Attenuates Neutrophilic Inflammation and Lung Dysfunction during Klebsiella
819 pneumoniae Infection in Mice. *International Journal of Molecular Sciences*, *23*(11), 6246.
820 https://doi.org/10.3390/ijms23116246
821 **6.** Bradley, H., Markowitz, L. E., Gibson, T., & McQuillan, G. M. (2014). Seroprevalence of
822 herpes simplex virus types 1 and 2—United States, 1999-2010. *The Journal of Infectious*
823 *Diseases*, *209*(3), 325–333. https://doi.org/10.1093/infdis/jit458
824 **7.** Broggi, A., Granucci, F., & Zanoni, I. (2020). Type III interferons: Balancing tissue
825 tolerance and resistance to pathogen invasion. *The Journal of Experimental Medicine*,
826 *217*(1), e20190295. https://doi.org/10.1084/jem.20190295
827 **8.** Broggi, A., Tan, Y., Granucci, F., & Zanoni, I. (2017). IFN-λ suppresses intestinal
828 inflammation by non-translational regulation of neutrophil function. *Nature Immunology*,
829 *18*(10), 1084–1093. https://doi.org/10.1038/ni.3821
830 **9.** Caine, E. A., Scheaffer, S. M., Arora, N., Zaitsev, K., Artyomov, M. N., Coyne, C. B.,
831 Moley, K. H., & Diamond, M. S. (2019). Interferon lambda protects the female
832 reproductive tract against Zika virus infection. *Nature Communications*, *10*(1), 280.
833 https://doi.org/10.1038/s41467-018-07993-2

834 **10.** Casazza, R. L., Philip, D. T., & Lazear, H. M. (2022). Interferon Lambda Signals in
835 Maternal Tissues to Exert Protective and Pathogenic Effects in a Gestational Stage-
836 Dependent Manner. *MBio*, *13*(3), e0385721. https://doi.org/10.1128/mbio.03857-21
837 **11.** Chami, B., Yeung, A., Buckland, M., Liu, H., M. Fong, G., Tao, K., & Bao, S. (2017).
838 CXCR3 plays a critical role for host protection against Salmonellosis. *Scientific Reports*,
839 *7*(1), Article 1. https://doi.org/10.1038/s41598-017-09150-z
840 **12.** Chami, B., Yeung, A. W. S., van Vreden, C., King, N. J. C., & Bao, S. (2014). The role of
841 CXCR3 in DSS-induced colitis. *PloS One*, *9*(7), e101622.
842 https://doi.org/10.1371/journal.pone.0101622
843 **13.** Coldbeck-Shackley, R. C., Romeo, O., Rosli, S., Gearing, L. J., Gould, J. A., Lim, S. S.,
844 Van der Hoek, K. H., Eyre, N. S., Shue, B., Robertson, S. A., Best, S. M., Tate, M. D.,
845 Hertzog, P. J., & Beard, M. R. (2023). Constitutive expression and distinct properties of
846 IFN-epsilon protect the female reproductive tract from Zika virus infection. *PLoS*
847 *Pathogens*, *19*(3), e1010843. https://doi.org/10.1371/journal.ppat.1010843
848 **14.** Dinnon, K. H., Leist, S. R., Schäfer, A., Edwards, C. E., Martinez, D. R., Montgomery, S.
849 A., West, A., Yount, B. L., Hou, Y. J., Adams, L. E., Gully, K. L., Brown, A. J., Huang, E.,
850 Bryant, M. D., Choong, I. C., Glenn, J. S., Gralinski, L. E., Sheahan, T. P., & Baric, R. S.
851 (2020). A mouse-adapted model of SARS-CoV-2 to test COVID-19 countermeasures.
852 *Nature*, *586*(7830), 560–566. https://doi.org/10.1038/s41586-020-2708-8
853 **15.** Douam, F., Soto Albrecht, Y. E., Hrebikova, G., Sadimin, E., Davidson, C., Kotenko, S.
854 V., & Ploss, A. (2017). Type III Interferon-Mediated Signaling Is Critical for Controlling
855 Live Attenuated Yellow Fever Virus Infection In Vivo. *MBio*, *8*(4), e00819-17.
856 https://doi.org/10.1128/mBio.00819-17
857 **16.** Dowling, J. W., & Forero, A. (2022). Beyond Good and Evil: Molecular Mechanisms of
858 Type I and III IFN Functions. *Journal of Immunology (Baltimore, Md.: 1950)*, *208*(2),
859 247–256. https://doi.org/10.4049/jimmunol.2100707

17. Eichelberger, K. R., Jones, G. S., & Goldman, W. E. (2019). Inhibition of Neutrophil Primary Granule Release during Yersinia pestis Pulmonary Infection. *MBio*, *10*(6), e02759-19. https://doi.org/10.1128/mBio.02759-19

18. Espinosa, V., Dutta, O., Mc Elrath, C., Du, P., Chang, Y.-J., Cicciarelli, B., Pitler, A., Whitehead, I., Obar, J. J., Durbin, J., Kotenko, S., & Rivera, A. (2017). Type III interferon is a critical regulator of innate antifungal immunity. *Science Immunology*, *2*(16), eaan5357. https://doi.org/10.1126/sciimmunol.aan5357

19. Feld, J. J., Kandel, C., Biondi, M. J., Kozak, R. A., Zahoor, M. A., Lemieux, C., Borgia, S. M., Boggild, A. K., Powis, J., McCready, J., Tan, D. H. S., Chan, T., Coburn, B., Kumar, D., Humar, A., Chan, A., O'Neil, B., Noureldin, S., Booth, J., … Hansen, B. E. (2021). Peginterferon lambda for the treatment of outpatients with COVID-19: A phase 2, placebo-controlled randomised trial. *The Lancet. Respiratory Medicine*, *9*(5), 498–510. https://doi.org/10.1016/S2213-2600(20)30566-X

20. Flisiak, R., Shiffman, M., Arenas, J., Cheinquer, H., Nikitin, I., Dong, Y., Rana, K., & Srinivasan, S. (2016). A Randomized Study of Peginterferon Lambda-1a Compared to Peginterferon Alfa-2a in Combination with Ribavirin and Telaprevir in Patients with Genotype-1 Chronic Hepatitis C. *PloS One*, *11*(10), e0164563. https://doi.org/10.1371/journal.pone.0164563

21. Forero, A., Ozarkar, S., Li, H., Lee, C. H., Hemann, E. A., Nadjsombati, M. S., Hendricks, M. R., So, L., Green, R., Roy, C. N., Sarkar, S. N., von Moltke, J., Anderson, S. K., Gale, M., & Savan, R. (2019). Differential Activation of the Transcription Factor IRF1 Underlies the Distinct Immune Responses Elicited by Type I and Type III Interferons. *Immunity*, *51*(3), 451-464.e6. https://doi.org/10.1016/j.immuni.2019.07.007

22. Friedman, H. M., Macarak, E. J., MacGregor, R. R., Wolfe, J., & Kefalides, N. A. (1981). Virus infection of endothelial cells. *The Journal of Infectious Diseases*, *143*(2), 266–273. https://doi.org/10.1093/infdis/143.2.266

886 **23.** Galani, I. E., Triantafyllia, V., Eleminiadou, E.-E., Koltsida, O., Stavropoulos, A.,
887 Manioudaki, M., Thanos, D., Doyle, S. E., Kotenko, S. V., Thanopoulou, K., &
888 Andreakos, E. (2017). Interferon-λ Mediates Non-redundant Front-Line Antiviral
889 Protection against Influenza Virus Infection without Compromising Host Fitness.
890 *Immunity*, *46*(5), 875-890.e6. https://doi.org/10.1016/j.immuni.2017.04.025
891 **24.** Gharaee-Kermani, M., Estadt, S. N., Tsoi, L. C., Wolf-Fortune, S. J., Liu, J., Xing, X.,
892 Theros, J., Reed, T. J., Lowe, L., Gruszka, D., Ward, N. L., Gudjonsson, J. E., &
893 Kahlenberg, J. M. (2022). IFN-κ Is a Rheostat for Development of Psoriasiform
894 Inflammation. *The Journal of Investigative Dermatology*, *142*(1), 155-165.e3.
895 https://doi.org/10.1016/j.jid.2021.05.029
896 **25.** Goel, R. R., Wang, X., O'Neil, L. J., Nakabo, S., Hasneen, K., Gupta, S., Wigerblad, G.,
897 Blanco, L. P., Kopp, J. B., Morasso, M. I., Kotenko, S. V., Yu, Z.-X., Carmona-Rivera, C.,
898 & Kaplan, M. J. (2020). Interferon lambda promotes immune dysregulation and tissue
899 inflammation in TLR7-induced lupus. *Proceedings of the National Academy of Sciences*
900 *of the United States of America*, *117*(10), 5409–5419.
901 https://doi.org/10.1073/pnas.1916897117
902 **26.** Grau, K. R., Zhu, S., Peterson, S. T., Helm, E. W., Philip, D., Phillips, M., Hernandez, A.,
903 Turula, H., Frasse, P., Graziano, V. R., Wilen, C. B., Wobus, C. E., Baldridge, M. T., &
904 Karst, S. M. (2020). The intestinal regionalization of acute norovirus infection is
905 regulated by the microbiota via bile acid-mediated priming of type III interferon. *Nature*
906 *Microbiology*, *5*(1), 84–92. https://doi.org/10.1038/s41564-019-0602-7
907 **27.** Handfield, C., Kwock, J., & MacLeod, A. S. (2018). Innate Antiviral Immunity in the Skin.
908 *Trends in Immunology*, *39*(4), 328–340. https://doi.org/10.1016/j.it.2018.02.003
909 **28.** Hartl, D., Krauss-Etschmann, S., Koller, B., Hordijk, P. L., Kuijpers, T. W., Hoffmann, F.,
910 Hector, A., Eber, E., Marcos, V., Bittmann, I., Eickelberg, O., Griese, M., & Roos, D.
911 (2008). Infiltrated neutrophils acquire novel chemokine receptor expression and

912 chemokine responsiveness in chronic inflammatory lung diseases. *Journal of*
913 *Immunology (Baltimore, Md.: 1950)*, *181*(11), 8053–8067.
914 https://doi.org/10.4049/jimmunol.181.11.8053

915 **29.** Hemann, E. A., Green, R., Turnbull, J. B., Langlois, R. A., Savan, R., & Gale, M. (2019).
916 Interferon-λ modulates dendritic cells to facilitate T cell immunity during infection with
917 influenza A virus. *Nature Immunology*, *20*(8), 1035–1045.
918 https://doi.org/10.1038/s41590-019-0408-z

919 **30.** Hor, J. L., Heath, W. R., & Mueller, S. N. (2017). Neutrophils are dispensable in the
920 modulation of T cell immunity against cutaneous HSV-1 infection. *Scientific Reports*, *7*,
921 41091. https://doi.org/10.1038/srep41091

922 **31.** Jagger, B. W., Miner, J. J., Cao, B., Arora, N., Smith, A. M., Kovacs, A., Mysorekar, I. U.,
923 Coyne, C. B., & Diamond, M. S. (2017). Gestational Stage and IFN-λ Signaling Regulate
924 ZIKV Infection In Utero. *Cell Host & Microbe*, *22*(3), 366-376.e3.
925 https://doi.org/10.1016/j.chom.2017.08.012

926 **32.** Karin, N. (2020). CXCR3 Ligands in Cancer and Autoimmunity, Chemoattraction of
927 Effector T Cells, and Beyond. *Frontiers in Immunology*, *11*, 976.
928 https://doi.org/10.3389/fimmu.2020.00976

929 **33.** Kawakami, Y., Ando, T., Lee, J.-R., Kim, G., Kawakami, Y., Nakasaki, T., Nakasaki, M.,
930 Matsumoto, K., Choi, Y. S., & Kawakami, T. (2017). Defective natural killer cell activity in
931 a mouse model of eczema herpeticum. *The Journal of Allergy and Clinical Immunology*,
932 *139*(3), 997-1006.e10. https://doi.org/10.1016/j.jaci.2016.06.034

933 **34.** Kobayashi, T., Naik, S., & Nagao, K. (2019). Choreographing immunity in the skin
934 epithelial barrier. *Immunity*, *50*(3), 552–565.
935 https://doi.org/10.1016/j.immuni.2019.02.023

936 **35.** Kollias, C. M., Huneke, R. B., Wigdahl, B., & Jennings, S. R. (2015). Animal models of
937 herpes simplex virus immunity and pathogenesis. *Journal of Neurovirology*, *21*(1), 8–23.
938 https://doi.org/10.1007/s13365-014-0302-2
939 **36.** LaFleur, D. W., Nardelli, B., Tsareva, T., Mather, D., Feng, P., Semenuk, M., Taylor, K.,
940 Buergin, M., Chinchilla, D., Roshke, V., Chen, G., Ruben, S. M., Pitha, P. M., Coleman,
941 T. A., & Moore, P. A. (2001). Interferon-kappa, a novel type I interferon expressed in
942 human keratinocytes. *The Journal of Biological Chemistry*, *276*(43), 39765–39771.
943 https://doi.org/10.1074/jbc.M102502200
944 **37.** Lazear, H. M., Daniels, B. P., Pinto, A. K., Huang, A. C., Vick, S. C., Doyle, S. E., Gale,
945 M., Klein, R. S., & Diamond, M. S. (2015). Interferon-λ restricts West Nile virus
946 neuroinvasion by tightening the blood-brain barrier. *Science Translational Medicine*,
947 *7*(284), 284ra59. https://doi.org/10.1126/scitranslmed.aaa4304
948 **38.** Lazear, H. M., Schoggins, J. W., & Diamond, M. S. (2019). Shared and Distinct
949 Functions of Type I and Type III Interferons. *Immunity*, *50*(4), 907–923.
950 https://doi.org/10.1016/j.immuni.2019.03.025
951 **39.** Lebratti, T., Lim, Y. S., Cofie, A., Andhey, P., Jiang, X., Scott, J., Fabbrizi, M. R.,
952 Ozantürk, A. N., Pham, C., Clemens, R., Artyomov, M., Dinauer, M., & Shin, H. (2021). A
953 sustained type I IFN-neutrophil-IL-18 axis drives pathology during mucosal viral
954 infection. *ELife*, *10*, e65762. https://doi.org/10.7554/eLife.65762
955 **40.** Li, F., Adase, C. A., & Zhang, L. (2017). Isolation and Culture of Primary Mouse
956 Keratinocytes from Neonatal and Adult Mouse Skin. *Journal of Visualized Experiments :*
957 *JoVE*, *125*, 56027. https://doi.org/10.3791/56027
958 **41.** Lopez, C. A., Dulson, S. J., & Lazear, H. M. (2022). Zika Virus Replicates in the Vagina
959 of Mice with Intact Interferon Signaling. *Journal of Virology*, *96*(18), e0121922.
960 https://doi.org/10.1128/jvi.01219-22

961 **42.** Lou, F., Sun, Y., & Wang, H. (2020). Protocol for Flow Cytometric Detection of Immune
962 Cell Infiltration in the Epidermis and Dermis of a Psoriasis Mouse Model. *STAR*
963 *Protocols*, *1*(3), 100115. https://doi.org/10.1016/j.xpro.2020.100115
964 **43.** Ma, J. Z., Russell, T. A., Spelman, T., Carbone, F. R., & Tscharke, D. C. (2014). Lytic
965 Gene Expression Is Frequent in HSV-1 Latent Infection and Correlates with the
966 Engagement of a Cell-Intrinsic Transcriptional Response. *PLoS Pathogens*, *10*(7),
967 e1004237. https://doi.org/10.1371/journal.ppat.1004237
968 **44.** Mesev, E. V., LeDesma, R. A., & Ploss, A. (2019). Decoding type I and III interferon
969 signalling during viral infection. *Nature Microbiology*, *4*(6), 914–924.
970 https://doi.org/10.1038/s41564-019-0421-x
971 **45.** Miner, J. J., Platt, D. J., Ghaznavi, C. M., Chandra, P., Santeford, A., Menos, A. M.,
972 Dong, Z., Wang, E. R., Qian, W., Karozichian, E. S., Philips, J. A., & Apte, R. S. (2020).
973 HSV-1 and Zika Virus but Not SARS-CoV-2 Replicate in the Human Cornea and Are
974 Restricted by Corneal Type III Interferon. *Cell Reports*, *33*(5), 108339.
975 https://doi.org/10.1016/j.celrep.2020.108339
976 **46.** Muir, A. J., Arora, S., Everson, G., Flisiak, R., George, J., Ghalib, R., Gordon, S. C.,
977 Gray, T., Greenbloom, S., Hassanein, T., Hillson, J., Horga, M. A., Jacobson, I. M.,
978 Jeffers, L., Kowdley, K. V., Lawitz, E., Lueth, S., Rodriguez-Torres, M., Rustgi, V., …
979 EMERGE study group. (2014). A randomized phase 2b study of peginterferon lambda-
980 1a for the treatment of chronic HCV infection. *Journal of Hepatology*, *61*(6), 1238–1246.
981 https://doi.org/10.1016/j.jhep.2014.07.022
982 **47.** Nestle, F. O., Di Meglio, P., Qin, J.-Z., & Nickoloff, B. J. (2009). Skin immune sentinels in
983 health and disease. *Nature Reviews. Immunology*, *9*(10), 679–691.
984 https://doi.org/10.1038/nri2622

985 **48.** Novais, F. O., Amorim, C. F., & Scott, P. (2021). Host-Directed Therapies for Cutaneous
986 Leishmaniasis. *Frontiers in Immunology*, *12*, 660183.
987 https://doi.org/10.3389/fimmu.2021.660183
988 **49.** Peterson, S. T., Kennedy, E. A., Brigleb, P. H., Taylor, G. M., Urbanek, K., Bricker, T. L.,
989 Lee, S., Shin, H., Dermody, T. S., Boon, A. C. M., & Baldridge, M. T. (2019). Disruption
990 of Type III Interferon (IFN) Genes Ifnl2 and Ifnl3 Recapitulates Loss of the Type III IFN
991 Receptor in the Mucosal Antiviral Response. *Journal of Virology*, *93*(22), e01073-19.
992 https://doi.org/10.1128/JVI.01073-19
993 **50.** Phillipson, M., Heit, B., Colarusso, P., Liu, L., Ballantyne, C. M., & Kubes, P. (2006).
994 Intraluminal crawling of neutrophils to emigration sites: A molecularly distinct process
995 from adhesion in the recruitment cascade. *The Journal of Experimental Medicine*,
996 *203*(12), 2569–2575. https://doi.org/10.1084/jem.20060925
997 **51.** Reed, J. L., Scott, D. E., & Bray, M. (2012). Eczema vaccinatum. *Clinical Infectious*
998 *Diseases: An Official Publication of the Infectious Diseases Society of America*, *54*(6),
999 832–840. https://doi.org/10.1093/cid/cir952
1000 **52.** Sakamoto, K., Goel, S., Funakoshi, A., Honda, T., & Nagao, K. (2021). Flow cytometry
1001 analysis of the subpopulations of mouse keratinocytes and skin immune cells. *STAR*
1002 *Protocols*, *3*(1), 101052. https://doi.org/10.1016/j.xpro.2021.101052
1003 **53.** Santer, D. M., Minty, G. E. S., Golec, D. P., Lu, J., May, J., Namdar, A., Shah, J., Elahi,
1004 S., Proud, D., Joyce, M., Tyrrell, D. L., & Houghton, M. (2020). Differential expression of
1005 interferon-lambda receptor 1 splice variants determines the magnitude of the antiviral
1006 response induced by interferon-lambda 3 in human immune cells. *PLoS Pathogens*,
1007 *16*(4), e1008515. https://doi.org/10.1371/journal.ppat.1008515
1008 **54.** Shmeleva, E. V., Gomez de Agüero, M., Wagner, J., Enright, A. J., Macpherson, A. J.,
1009 Ferguson, B. J., & Smith, G. L. (2022). Smallpox vaccination induces a substantial
1010 increase in commensal skin bacteria that promote pathology and influence the host

response. *PLoS Pathogens*, *18*(4), e1009854. https://doi.org/10.1371/journal.ppat.1009854

55. Simmons, A., & Nash, A. A. (1984). Zosteriform spread of herpes simplex virus as a model of recrudescence and its use to investigate the role of immune cells in prevention of recurrent disease. *Journal of Virology*, *52*(3), 816–821.

56. van Lint, A., Ayers, M., Brooks, A. G., Coles, R. M., Heath, W. R., & Carbone, F. R. (2004). Herpes simplex virus-specific CD8+ T cells can clear established lytic infections from skin and nerves and can partially limit the early spread of virus after cutaneous inoculation. *Journal of Immunology (Baltimore, Md.: 1950)*, *172*(1), 392–397. https://doi.org/10.4049/jimmunol.172.1.392

57. Wang, P., Gamero, A. M., & Jensen, L. E. (2019). IL-36 promotes anti-viral immunity by boosting sensitivity to IFN-α/β in IRF1 dependent and independent manners. *Nature Communications*, *10*(1), 4700. https://doi.org/10.1038/s41467-019-12318-y

58. Wharton, M., Strikas, R. A., Harpaz, R., Rotz, L. D., Schwartz, B., Casey, C. G., Pearson, M. L., Anderson, L. J., Advisory Committee on Immunization Practices, & Healthcare Infection Control Practices Advisory Committee. (2003). Recommendations for using smallpox vaccine in a pre-event vaccination program. Supplemental recommendations of the Advisory Committee on Immunization Practices (ACIP) and the Healthcare Infection Control Practices Advisory Committee (HICPAC). *MMWR. Recommendations and Reports: Morbidity and Mortality Weekly Report. Recommendations and Reports*, *52*(RR-7), 1–16.

59. Wojtasiak, M., Pickett, D. L., Tate, M. D., Bedoui, S., Job, E. R., Whitney, P. G., Brooks, A. G., & Reading, P. C. (2010). Gr-1+ cells, but not neutrophils, limit virus replication and lesion development following flank infection of mice with herpes simplex virus type-1. *Virology*, *407*(1), 143–151. https://doi.org/10.1016/j.virol.2010.08.001

1036 **60.** Wolk, K., Witte, K., Witte, E., Raftery, M., Kokolakis, G., Philipp, S., Schönrich, G.,
1037 Warszawska, K., Kirsch, S., Prösch, S., Sterry, W., Volk, H.-D., & Sabat, R. (2013). IL-29
1038 is produced by T(H)17 cells and mediates the cutaneous antiviral competence in
1039 psoriasis. *Science Translational Medicine*, *5*(204), 204ra129.
1040 https://doi.org/10.1126/scitranslmed.3006245
1041 **61.** Wollenberg, A., Wetzel, S., Burgdorf, W. H. C., & Haas, J. (2003). Viral infections in
1042 atopic dermatitis: Pathogenic aspects and clinical management. *The Journal of Allergy*
1043 *and Clinical Immunology*, *112*(4), 667–674. https://doi.org/10.1016/j.jaci.2003.07.001
1044 **62.** Ye, L., Schnepf, D., Becker, J., Ebert, K., Tanriver, Y., Bernasconi, V., Gad, H. H.,
1045 Hartmann, R., Lycke, N., & Staeheli, P. (2019). Interferon-λ enhances adaptive mucosal
1046 immunity by boosting release of thymic stromal lymphopoietin. *Nature Immunology*,
1047 *20*(5), 593–601. https://doi.org/10.1038/s41590-019-0345-x
1048 **63.** Zenaro, E., Pietronigro, E., Della Bianca, V., Piacentino, G., Marongiu, L., Budui, S.,
1049 Turano, E., Rossi, B., Angiari, S., Dusi, S., Montresor, A., Carlucci, T., Nanì, S.,
1050 Tosadori, G., Calciano, L., Catalucci, D., Berton, G., Bonetti, B., & Constantin, G. (2015).
1051 Neutrophils promote Alzheimer's disease-like pathology and cognitive decline via LFA-1
1052 integrin. *Nature Medicine*, *21*(8), 880–886. https://doi.org/10.1038/nm.3913
1053 **64.** Zhou, Z., Hamming, O. J., Ank, N., Paludan, S. R., Nielsen, A. L., & Hartmann, R.
1054 (2007). Type III interferon (IFN) induces a type I IFN-like response in a restricted subset
1055 of cells through signaling pathways involving both the Jak-STAT pathway and the
1056 mitogen-activated protein kinases. *Journal of Virology*, *81*(14), 7749–7758.
1057 https://doi.org/10.1128/JVI.02438-06

1058

1059 **FIGURE LEGENDS**

1060 **Figure 1. IFN-λ signaling protects against severe HSV skin disease without affecting viral**
1061 **replication. A-E.** 8-12 week-old male and female WT and *Ifnlr1*$^{-/-}$ mice were infected with 10^6 FFU

of HSV-1 strain NS. **A**. Dermatome skin lesions were photographed 6 dpi. **B.** HSV-1 skin lesions were measured from photographs 6, 8, and 10 dpi using imageJ. **C.** Skin lesion severity was categorized based on 6 dpi lesion area. **D.** Skin viral loads were measured 2-10 dpi by focus-forming assay. **E.** Viral loads in ipsilateral and contralateral dorsal root ganglia (L2-L5 pooled for each mouse) were measured by qPCR. **F-G.** 8-12 week-old male and female WT and *Ifnlr1*$^{-/-}$ mice were infected with 10^3 FFU of HSV-2 strain 333. **F.** Dermatome lesions photographed 8 dpi. **G.** HSV-2 skin lesions were measured from photographs 6 and 8 dpi using ImageJ. **H.** 8-12 week-old female WT and *Ifnlr1*$^{-/-}$ mice were infected with 10^3 FFU of HSV-2 strain 333 intravaginally and HSV-2 vaginal disease was scored 6-8dpi as follows: 1: mild redness and swelling, 2: visible ulceration and fur loss, 3: severe ulceration and signs of sickness, 4: hindlimb paralysis, 5: moribund/dead. Differences in lesion area and viral load were compared by Mann-Whitney U test. Differences in categorical skin disease were compared by Cochran-Armitage test. *P* values are reported with $P < 0.05$ considered to be statistically significant.

Figure 2. The protective effect of IFN-λ in the skin does not require IFN-α/β signaling. 8-12 week-old *Ifnar1*$^{-/-}$ and *Ifnar1*$^{-/-}$ *Ifnlr1*$^{-/-}$ DKO male and female mice were infected with 10^6 FFU of HSV-1. **A.** Lethality was monitored daily (n=15 *Ifnar1*$^{-/-}$ and 10 DKO mice). **B**. Dermatome skin lesions were photographed 4 dpi. **C.** Skin lesion areas were measured from photographs 4 dpi using ImageJ. **D.** Skin lesion severity was categorized based on 4 dpi lesion area. **E.** Skin viral loads were measured 2 and 4 dpi by focus-forming assay. Survival differences were compared by Mantel-Cox Log-Rank test. Differences in lesion area and viral load were compared by Mann-Whitney U test and differences in categorical skin disease were compared by Cochran-Armitage test. *P* values are reported with $P < 0.05$ considered to be statistically significant.

Figure 3. IFN-λ cytokines protect against severe HSV-1 skin disease. A-D. 8-12 week-old WT, *Ifnl2/3*$^{-/-}$, and *Ifnk*$^{-/-}$ male and female mice were infected with 10^6 FFU of HSV-1. **A**.

Dermatome skin lesions were photographed 6 dpi. **B.** Skin lesion areas were measured from photographs 6 dpi using ImageJ. **C.** Skin lesion severity was categorized based on 6 dpi lesion area. **D.** Skin viral loads were measured 6 dpi by FFA. **E-G.** 8 week-old WT and *Ifnl2/3*$^{-/-}$ male and female mice were lethally irradiated and transfused with 10^7 bone marrow cells from WT or *Ifnl2/3*$^{-/-}$ donors. 10 weeks later, mice were infected with 10^6 FFU of HSV-1. **E.** Skin lesion areas were measured from photographs 6 dpi using ImageJ. **F.** Skin lesion severity was categorized based upon 6 dpi lesion area. **G.** Skin viral loads were measured 6 dpi by FFA. **H-I.** 8-12 week-old WT male and female mice were depilated and then topically treated with 5 µg of recombinant murine IFN-λ3 or PBS. 24 hours later, mice were infected with 10^6 FFU of HSV-1 at the treated site. **H.** Skin lesion areas were measured from photographs 6 dpi using ImageJ. **I.** Skin viral loads were measured 6 dpi by FFA. Differences in lesion area and viral load were compared by Mann-Whitney U test and differences in categorical skin disease were compared by Cochran-Armitage test. *P* values are reported with $P < 0.05$ considered to be statistically significant.

Figure 4. IFN-λ signaling in both keratinocytes and leukocytes is necessary to restrict severe HSV-1 skin disease. 8-12 week-old male and female WT, *Ifnlr1*$^{-/-}$, *K14*-Cre-*Ifnlr1*$^{-/-}$, and *Vav*-Cre-*Ifnlr1*$^{-/-}$ mice were infected with 10^6 FFU of HSV-1. **A**. Dermatome skin lesions photographed were 6 dpi. **B.** Skin lesion areas were measured from photographs 6 dpi using ImageJ. **C.** Skin lesion severity was categorized based on 6 dpi lesion area. **D.** Skin viral loads were measured 6 dpi by FFA. Differences in lesion area and viral load were compared by Mann-Whitney U test and differences in categorical skin disease were compared by Cochran-Armitage test. *P* values are reported with $P < 0.05$ considered to be statistically significant.

Figure 5. IFN-λ signaling in keratinocytes differentially regulates CXCL9 induction. Primary keratinocytes were prepared from WT, *Ifnlr1*$^{-/-}$, *Ifnar1*$^{-/-}$, and *Ifnar1*$^{-/-}$ *Ifnlr1*$^{-/-}$ DKO mice and treated with IFN-λ3 (5 ng/mL), IFN-β (5 ng/mL), or media alone for 24 hours. **A.** RNA was extracted and

IFN-stimulated gene expression was measured by qRT-PCR. *Ifit1* expression is shown relative to *ActB* (housekeeping gene) and normalized to expression in media-treated WT cells. Results represent 6 samples from 2 independent experiments. **B-F.** RNA from 3 samples per genotype per treatment was analyzed by RNAseq (NovaSeq6000S4 XP Paired End 2x100). **B.** Principal component analysis for all analyzed samples. **C.** Volcano plots showing differentially expressed genes after IFN-λ or IFN-β treatment, compared to media-only treated keratinocytes. Differentially expressed genes were defined as having a $|Log_2Fold\ Change| > 1$ and an FDR p-value ≤ 0.05. **D.** Venn diagram showing DEGs induced by IFN-λ and IFN-β in WT or knockout keratinocytes. **E.** Table of IFN-λ-specific DEGs, their Log_2Fold Change, and FDR p-value for IFN-λ and IFN-β-treated WT keratinocytes. **F.** Volcano plot showing DEGs after IFN-λ treatment compared to IFN-β treatment in WT and receptor knockout keratinocytes.

Figure 6. IFN-λ signaling limits neutrophil abundance and severe skin pathology following HSV-1 infection. 8-12 week-old male and female WT and *Ifnlr1*$^{-/-}$ mice were infected with 10^6 FFU of HSV-1. **A-B.** Dermatome lesions and adjacent healthy skin were collected 4-8 dpi and analyzed by flow cytometry. **A.** Representative histogram of WT and *Ifnlr1*$^{-/-}$ lesions showing Ly6G+ neutrophil gating strategy (CD45+, CD11b+, Ly6G+) at 6 dpi. **B.** Frequency of neutrophils (Ly6G+ out of CD45+ CD11b+ live cells) for WT and *Ifnlr1*$^{-/-}$ dermatome lesions and adjacent healthy skin. Significant differences in neutrophil frequency were determined using an unpaired t test. *P* values are reported with $P < 0.05$ considered to be statistically significant. **C-D.** Inoculated flank skin was collected at 6 dpi and serial sections of the same skin lesion were processed for histology. **C.** H&E staining; black arrow denotes a neutrophilic pustule, red arrow denotes diffuse neutrophilic infiltrate. **D.** Anti-HSV-1 immunohistochemistry; viral antigen staining is denoted by black arrows. Scale bars are 100 μm.

Figure 7. IFN-λ signaling suppresses neutrophil-mediated pathology to limit HSV-1 skin disease. A. Experimental design for neutrophil depletions **B-D**. WT and *Ifnlr1*$^{-/-}$ mice were infected with 10^6 FFU of HSV-1. 0, 2, and 4 dpi mice were injected intraperitoneally with PBS, 250 µg of αIsotype control (IgG2a), or 250 µg of αLy6G (Clone 1A8). **B.** Spleens were harvested 6 dpi and analyzed by flow cytometry to confirm neutrophil depletion. **C.** Skin lesions were photographed 6 dpi and lesion areas measured ImageJ. **D.** Skin lesion severity was categorized based on 6 dpi lesion area. **E-G.** WT and *Ifnlr1*$^{-/-}$ mice were infected with 10^6 FFU of HSV-1 and 6 dpi skin lesions were photographed and analyzed via flow cytometry. **E.** Representative plots and gating strategy for neutrophil phenotyping markers LFA-1 and CD63 (% of CD45+ CD11b+ Ly6G+). **F.** Frequency of CD63+ neutrophils. **G.** Frequency of LFA-1+ CD63- neutrophils. Differences in lesion area and viral load were compared by Mann-Whitney U test and differences in categorical skin disease were compared by Cochran-Armitage test. Neutrophil frequencies were compared by unpaired t test. *P* values are reported with $P < 0.05$ considered to be statistically significant.

Figure 8. IFN-λ signaling in neutrophils contributes to protection from severe HSV-1 skin disease. 8-12 week-old male and female WT, *Ifnlr1*$^{-/-}$, *LysM*-Cre-*Ifnlr1*$^{-/-}$, and *Mrp8*-Cre-*Ifnlr1*$^{-/-}$ mice were infected with 10^6 FFU of HSV-1. **A**. Dermatome skin lesions were photographed 6 dpi. **B.** Skin lesion areas were measured from photographs 6 dpi using image J. **C.** Skin lesion severity was categorized based on 6 dpi lesion area. Differences in lesion area and viral load were compared by Mann-Whitney U test. Differences in categorical skin disease were compared by Cochran-Armitage test. *P* values are reported with $P < 0.05$ considered to be statistically significant.

Figure 9. IFN-λ signaling in keratinocytes restricts CXCL9 production to limit neutrophil recruitment and HSV-1 skin disease. 8-12 week-old male and female mice were infected with 10^6 FFU of HSV-1 and skin lesions were analyzed 6 dpi. **A.** CXCL9 was measured by ELISA in

homogenates of lesional skin or adjacent healthy skin from WT and *Ifnlr1*$^{-/-}$ mice. **B-D.** WT and *K14*-Cre-*Ifnlr1*$^{-/-}$ mice were infected with HSV-1 and injected intraperitoneally with anti-CXCL9 (300µg) or PBS 0, 2, and 4 dpi. Skin lesion areas were measured from photographs 6 dpi (**B**) and lesion severity categorized (**C**). **D.** Neutrophil frequency in skin lesions was measured by flow cytometry 6 dpi. Differences in lesion area and viral load were compared by Mann-Whitney U test. Differences in categorical skin disease were compared by Cochran-Armitage test. Differences in CXCL9 concentration and neutrophil frequency were compared by unpaired t test. *P* values are reported with $P < 0.05$ considered to be statistically significant.

Supplementary Figure 1. Optimizing an HSV-1 skin infection model. A. HSV-1 skin infection model. **B-G.** 8-12 week-old male and female wild-type (C57BL/6) mice were infected with 10^6 FFU of HSV-1 strain NS and dermatome lesions were analyzed 6 dpi. **B.** Mice were depilated by manual plucking or by shaving plus Nair 1 day prior to infection. **C-D.** Depilated right flank skin of mice was abraded prior to inoculation using 40 scratches with a 27G needle, 10 punctures with a Quintip allergy needle, or 1 puncture with a multi-pronged Greer pick allergy needle. **C.** Skin lesion viral loads were measured by FFA. **D.** Skin lesions were photographed and areas measured using ImageJ. **E-G.** 20 mice were depilated by manual plucking and infected 1 day later using a Quintip allergy needle. **E.** Skin lesions were photographed 6 dpi and lesion areas measured using ImageJ. The standard deviation of lesion areas was 12 mm^2. **F.** Lesion severity was categorized based on lesion area: <5 mm^2 = Mild, 5-23 mm^2 = Moderate, >23 mm^2 = Severe. **G.** Representative images of each skin disease severity category.

Supplementary Figure 2. Validation of keratinocyte-specific *Ifnlr1* conditional knockouts. Tissues (flank skin, blood, brain, spleen, tail) were harvested from 8-week-old *K14*-Cre- and *K14*-Cre+ littermates, both carrying homozygous floxed alleles of *Ifnlr1*. Cre and *Ifnlr1* genotyping was performed by PCR.

Supplementary Figure 3. Immunophenotyping of skin tissues from WT and *Ifnlr1*$^{-/-}$ mice. A. 8-12-week-old male and female WT and *Ifnlr1*$^{-/-}$ mice were infected with 10^6 FFU of HSV-1. Dermatome skin lesions and adjacent healthy skin were collected 6 dpi, processed to single cell suspensions, and analyzed by flow cytometry. All cell populations were normalized to the total live cell population in each sample (Zombie UV-). All leukocytes were CD45+ and the frequencies of leukocyte populations were determined as follows: γδ T cells (CD3+, γδTCR+), CD4 T cells (CD3+, CD4+), CD8 T cells (CD3+, CD8+), B Cells (CD3-, CD19+), dendritic cells (CD11c+; DC), activated macrophages (CD11b+, Ly6G-, Ly6C high), and NK cells (NK1.1+). Differences in leukocyte populations were compared by unpaired t test, with $P < 0.05$ considered to be significant. These mice are the same as those in Fig. 6. **B.** Representative gating strategy to define neutrophil populations.

Supplementary Figure 4. IFN-λ and IFN-β induced transcriptional responses in A549 cells. *IFNLR1*$^{-/-}$, *IFNAR1*$^{-/-}$, and control (renilla luciferase) A549 cells were treated with IFN-λ2 (50 ng/mL), IFN-β (5 ng/mL), or media for 8 hours. **A.** RNA was extracted and IFN-stimulated gene expression was measured by qRT-PCR. *IFIT1* expression is shown relative to *ACTB* (housekeeping gene) and normalized to expression in media-treated Ren-Luc cells. Results represent 3 samples from one experiment. **B-F.** RNA was analyzed by RNAseq (NovaSeq6000S4 XP Paired End 2x100). **B.** Principal component analysis for all analyzed samples. **C.** Volcano plots showing differentially expressed genes after IFN-λ or IFN-β treatment, compared to media-only treated cells. Differentially expressed genes were defined as having a $|\text{Log}_2\text{Fold Change}| > 1$ and an FDR p-value ≤ 0.05. **D.** Venn diagram showing DEGs induced by IFN-λ and IFN-β in control or knockout cells. **E.** Table of IFN-λ-specific DEGs, their Log_2Fold

1215 Change, and FDR p-value for IFN-λ and IFN-β-treated control cells. **F.** Volcano plots showing

1216 DEGs after IFN-λ treatment compared to IFN-β treatment in control and receptor knockout cells.

1217

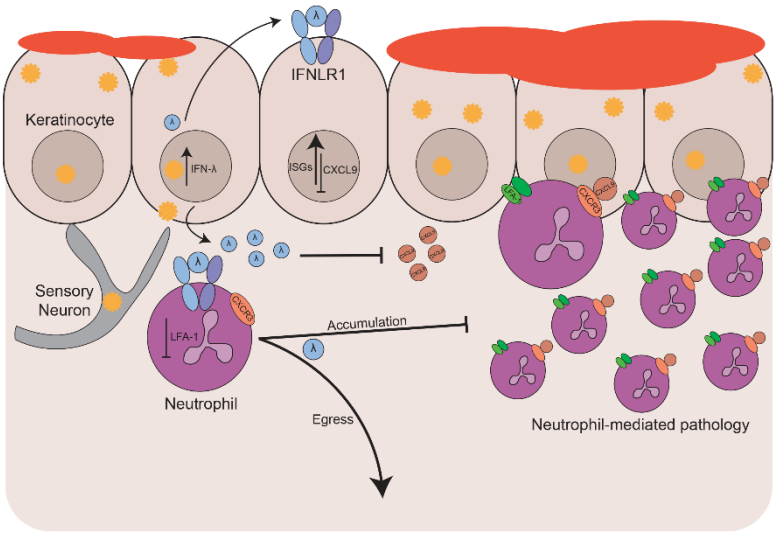

1218 **Graphical Abstract**

1219

1220

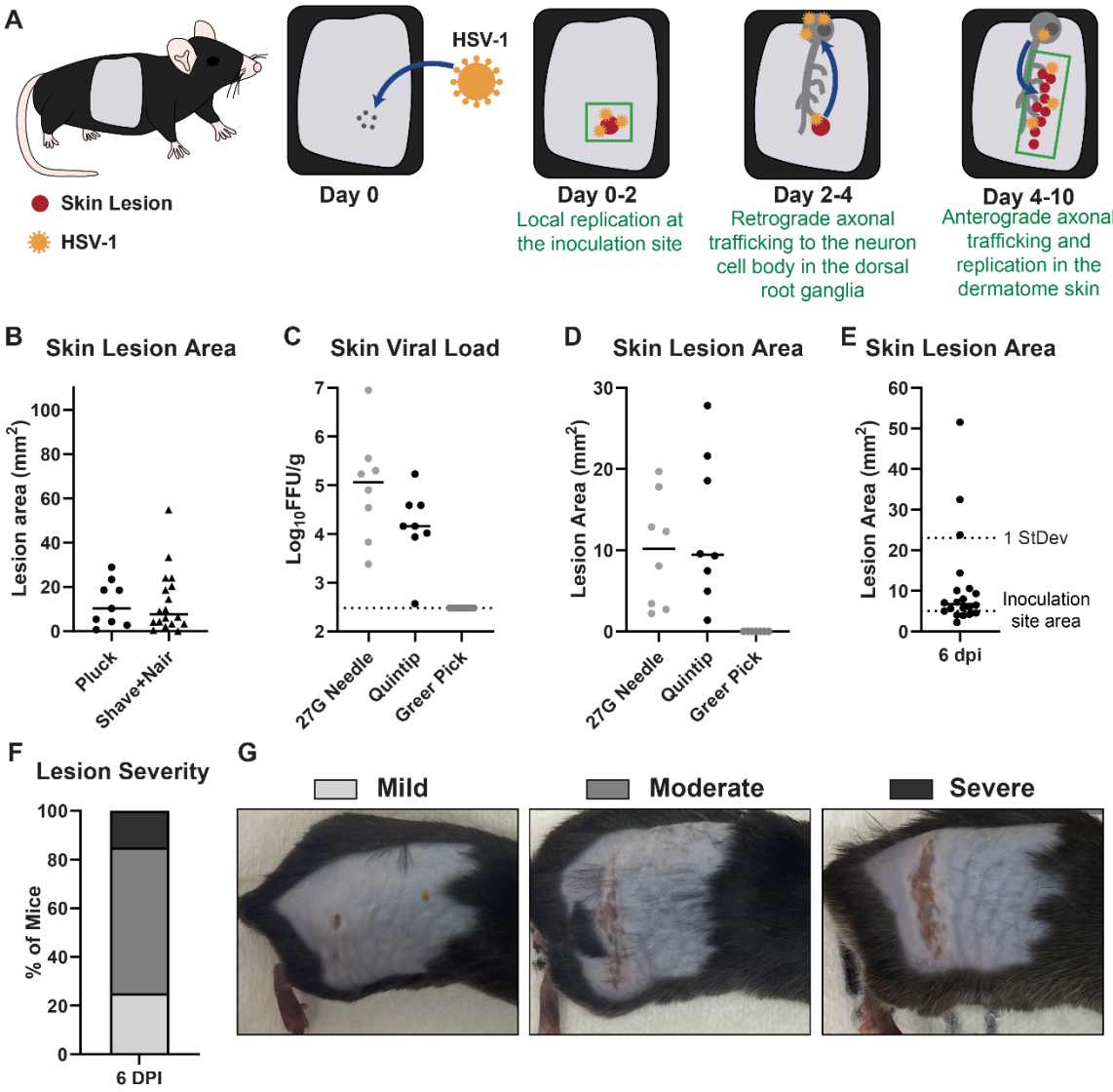

Supplementary Figure 1. Optimizing an HSV-1 skin infection model. A. HSV-1 skin infection model. **B-G.** 8-12 week-old male and female wild-type (C57BL/6) mice were infected with 10^6 FFU of HSV-1 strain NS and dermatome lesions were analyzed 6 dpi. **B.** Mice were depilated by manual plucking or by shaving plus Nair 1 day prior to infection. **C-D.** Depilated right flank skin of mice was abraded prior to inoculation using 40 scratches with a 27G needle, 10 punctures with a Quintip allergy needle, or 1 puncture with a multi-pronged Greer pick allergy needle. **C.** Skin lesion viral loads were measured by FFA. **D.** Skin lesions were photographed and areas measured using ImageJ. **E-G.** 20 mice were depilated by manual plucking and infected 1 day later using a Quintip allergy needle. **E.** Skin lesions were photographed 6 dpi and lesion areas measured using ImageJ. The standard deviation of lesion areas was 12 mm². **F.** Lesion severity was categorized based on lesion area: <5 mm² = Mild, 5-23 mm² = Moderate, >23 mm² = Severe. **G.** Representative images of each skin disease severity category.

1221

1222

1223

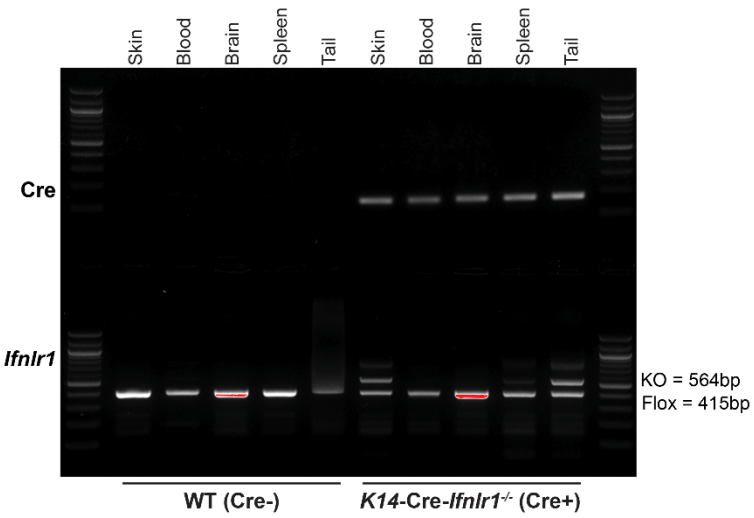

Supplementary Figure 2. Validation of keratinocyte-specific *Ifnlr1* conditional knockouts. Tissues (flank skin, blood, brain, spleen, tail) were harvested from 8-week-old *K14*-Cre- and *K14*-Cre+ littermates, both carrying homozygous floxed alleles of *Ifnlr1*. Cre and *Ifnlr1* genotyping was performed by PCR.

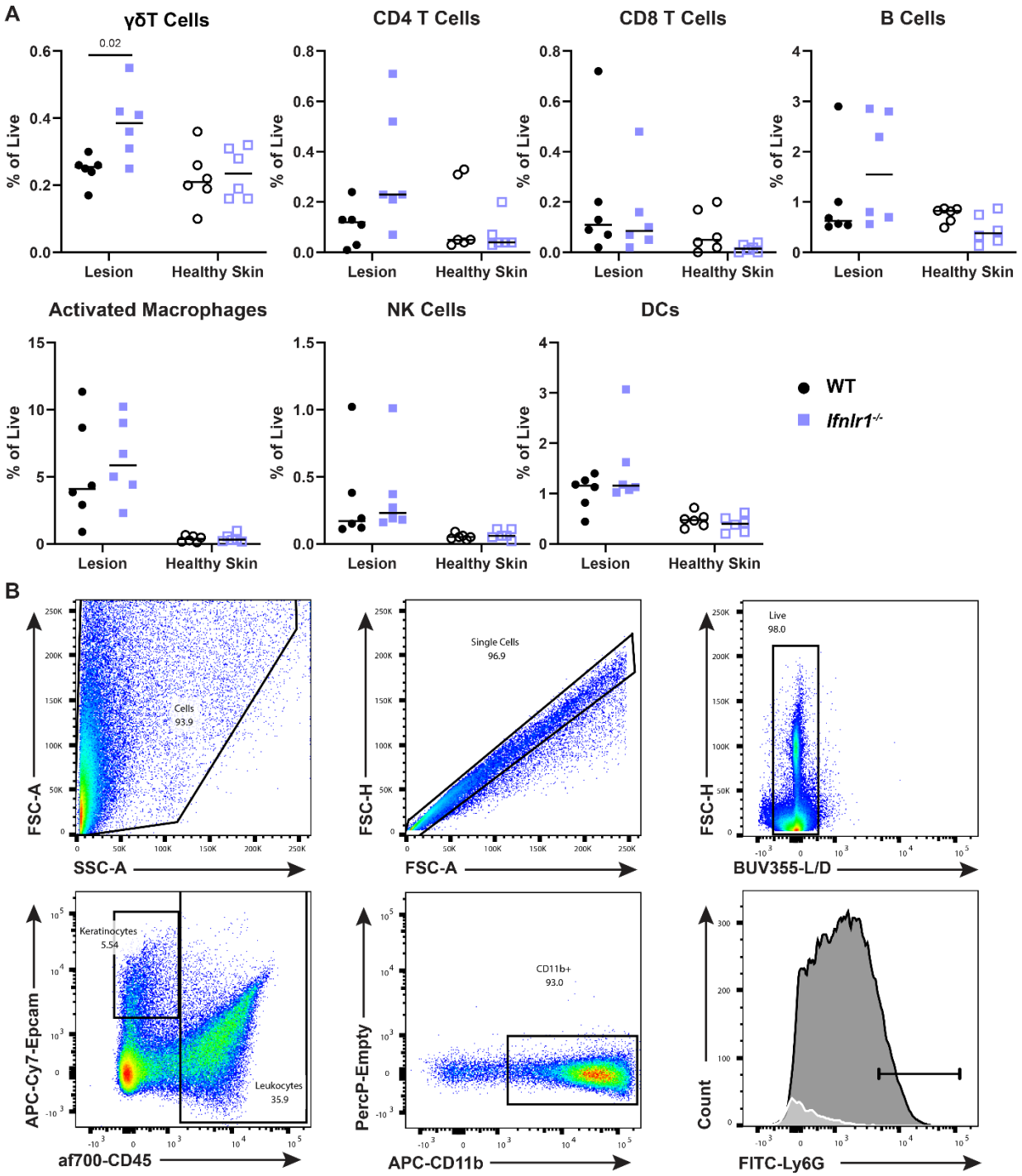

Supplementary Figure 3. Immunophenotyping of skin tissues from WT and *Ifnlr1*$^{-/-}$ mice. A. 8-12-week-old male and female WT and *Ifnlr1*$^{-/-}$ mice were infected with 10^6 FFU of HSV-1. Dermatome skin lesions and adjacent healthy skin were collected 6 dpi, processed to single cell suspensions, and analyzed by flow cytometry. All cell populations were normalized to the total live cell population in each sample (Zombie UV-). All leukocytes were CD45+ and the frequencies of leukocyte populations were determined as follows: γδ T cells (CD3+, γδTCR+), CD4 T cells (CD3+, CD4+), CD8 T cells (CD3+, CD8+), B Cells (CD3-, CD19+), dendritic cells (CD11c+; DC), activated macrophages (CD11b+, Ly6G-, Ly6C high), and NK cells (NK1.1+). Differences in leukocyte populations were compared by unpaired t test, with $P < 0.05$ considered to be significant. These mice are the same as those in Fig. 6. **B.** Representative gating strategy to define neutrophil populations.

1224

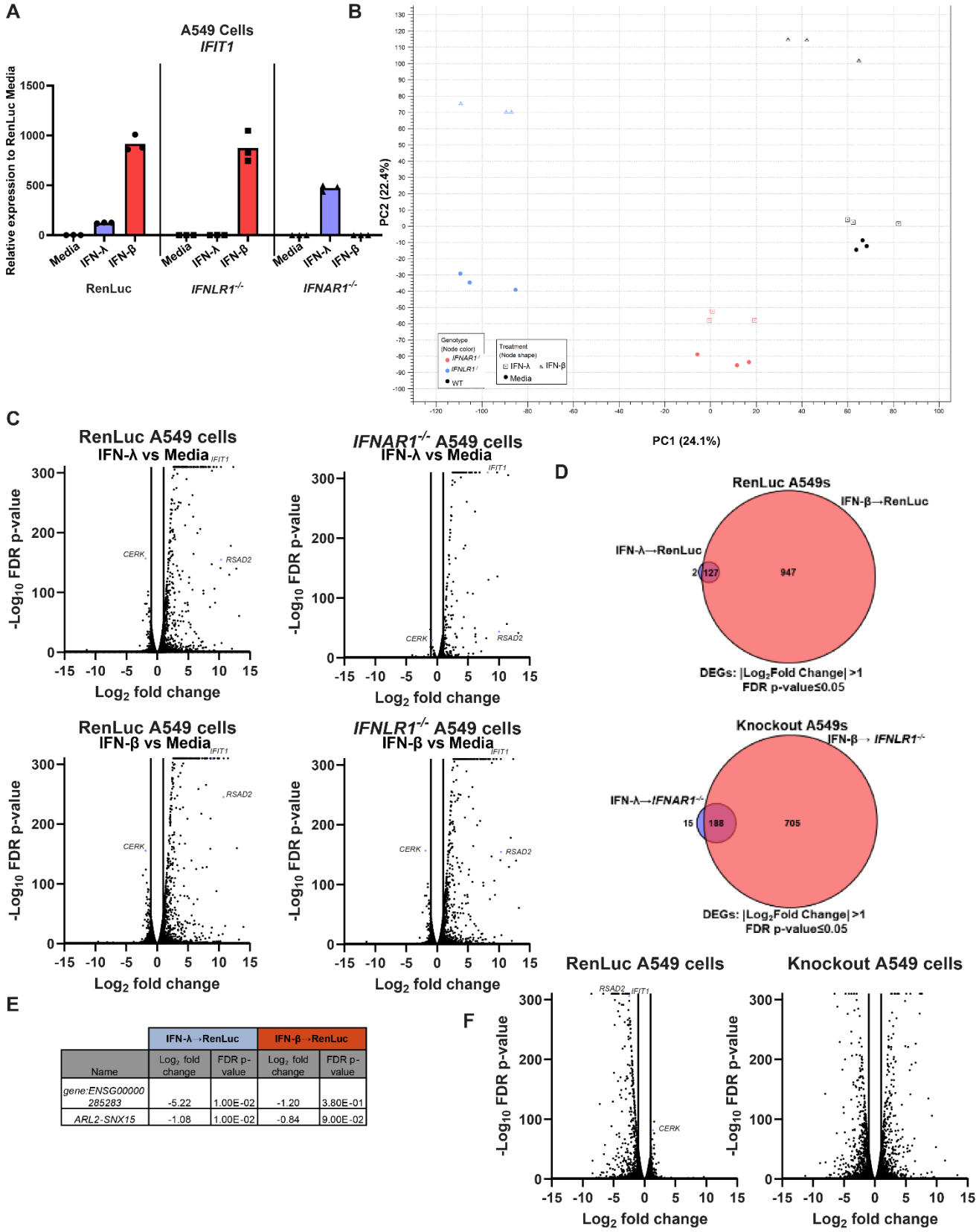

	IFN-λ →RenLuc		IFN-β →RenLuc	
Name	Log_2 fold change	FDR p-value	Log_2 fold change	FDR p-value
gene:ENSG00000285283	-5.22	1.00E-02	-1.20	3.80E-01
ARL2-SNX15	-1.08	1.00E-02	-0.84	9.00E-02

Supplementary Figure 4. IFN-λ and IFN-β induced transcriptional responses in A549 cells. *IFNLR1*$^{-/-}$, *IFNAR1*$^{-/-}$, and control (renilla luciferase) A549 cells were treated with IFN-λ2 (50 ng/mL), IFN-β (5 ng/mL), or media for 8 hours. **A.** RNA was extracted and IFN-stimulated gene expression was measured by qRT-PCR. *IFIT1* expression is shown relative to *ACTB* (housekeeping gene) and normalized to expression in media-treated Ren-Luc cells. Results represent 3 samples from one experiment. **B-F.** RNA was analyzed by RNAseq (NovaSeq6000S4 XP Paired End 2x100). **B.** Principal component analysis for all analyzed samples. **C.** Volcano plots showing differentially expressed genes after IFN-λ or IFN-β treatment, compared to media-only treated cells. Differentially expressed genes were defined as having a |Log_2Fold Change| >1 and an FDR p-value ≤ 0.05. **D.** Venn diagram showing DEGs induced by IFN-λ and IFN-β in control or knockout cells. **E.** Table of IFN-λ-specific DEGs, their Log_2Fold Change, and FDR p-value for IFN-λ and IFN-β-treated control cells. **F.** Volcano plots showing DEGs after IFN-λ treatment compared to IFN-β treatment in control and receptor knockout cells.